Check for updates

AGU ADVANCING EARTH AND SPACE SCIENCES

Earth and Space Science

RESEARCH ARTICLE
10.1029/2025EA004557

Special Collection:
The Lunar Trailblazer Mission Collection: Mission, Instruments, Data Analysis Plan

Visible-Shortwave Infrared (VSWIR) Spectral Parameters for the Lunar Trailblazer High-Resolution Volatiles and Minerals Moon Mapper (HVM^3)

Angela M. Dapremont[1], Rachel L. Klima[1], Kierra A. Wilk[2,3], Bethany L. Ehlmann[4], Christopher S. Edwards[5], Kerri L. Donaldson Hanna[6], Valeriya Kachmar[4], Laura Lee[5], Jasper K. Miura[4], Carlé M. Pieters[2], Erin Pimentel[4], Katherine A. Shirley[7], David R. Thompson[8], and Isabelle Adamczewski[4]

[1]Johns Hopkins University Applied Physics Laboratory, Laurel, MD, USA, [2]Brown University, Providence, RI, USA, [3]NASA Goddard Space Flight Center, Greenbelt, MD, USA, [4]California Institute of Technology, Pasadena, CA, USA, [5]Northern Arizona University, Flagstaff, AZ, USA, [6]University of Central Florida, Orlando, FL, USA, [7]Oxford University, Oxford, UK, [8]Jet Propulsion Laboratory, California Institute of Technology, Pasadena, CA, USA

Abstract The Lunar Trailblazer smallsat mission High-resolution Volatiles and Minerals Moon Mapper (HVM^3) science instrument was designed to acquire targeted spectral image cubes of the lunar surface at visible to shortwave infrared (VSWIR) wavelengths (0.6–3.6 μm) in an effort to understand the distribution, abundance, and form (OH, H_2O, ice) of lunar water, as well as the lunar water cycle. The Lunar Trailblazer mission end was declared in July 2025. Here, we describe the formulation and testing of VSWIR spectral parameters in preparation for previously anticipated returned data from HVM^3 using global image cubes and mosaic data from the Moon Mineralogy Mapper (M^3) imaging spectrometer, HVM^3's predecessor, and the Deep Impact spacecraft. We expand upon the existing M^3 global spectral parameter library, test the efficacy of presented parameters individually and alongside existing M^3 spectral parameters, provide examples of quantitative thresholds intended to indicate robust mineral detections, and discuss the spectral parameter limitations. We demonstrate that newly formulated and existing parameters capture lunar mineral diversity well and serve as a reliable indicator of lunar surface hydration, making them useful for existing and future scientific analysis using lunar orbital remote sensing data sets.

Plain Language Summary The High-resolution Volatiles and Minerals Moon Mapper (HVM^3) is one of two science instruments on the Lunar Trailblazer smallsat mission, whose science goal is to understand the distribution, abundance, and form of water on the Moon, as well as the lunar water cycle. HVM^3 uses patterns in infrared light reflection and absorption at different wavelengths to detect water and minerals in rocks and soils on the Moon's surface. In July 2025 the Lunar Trailblazer mission end was declared. Here, we detail the formulation and testing of algorithms for making water and mineral maps in preparation for the anticipated HVM^3 returned data using existing Moon Mineralogy Mapper (M^3) and Deep Impact spacecraft lunar data sets, which are similar types of instruments. We demonstrate that presented spectral parameters can distinguish lunar minerals of interest and therefore, capture lunar mineral diversity well. We also show that a newly developed water spectral parameter can be used as a reliable indication of lunar surface water presence, thereby demonstrating the value of expected HVM^3 maps for the broader scientific community as well as planning future exploration of the Moon.

Key Points:

- Legacy M^3 and updated visible-shortwave infrared spectral parameters were formulated and tested for the Lunar Trailblazer mission
- Spectral parameters capture lunar mineral diversity well and are readily distinguished particularly in conjunction with each other
- A newly presented water parameter serves as a reliable indicator of lunar surface hydration

Correspondence to:
A. M. Dapremont,
Angela.Dapremont@jhuapl.edu

Citation:
Dapremont, A. M., Klima, R. L., Wilk, K. A., Ehlmann, B. L., Edwards, C. S., Donaldson Hanna, K. L., et al. (2026). Visible-shortwave infrared (VSWIR) spectral parameters for the lunar trailblazer high-resolution volatiles and minerals Moon mapper (HVM^3). *Earth and Space Science*, *13*, e2025EA004557. https://doi.org/10.1029/2025EA004557

Received 24 JUN 2025
Accepted 3 DEC 2025

Author Contributions:
Conceptualization: Angela M. Dapremont, Rachel L. Klima, Kierra A. Wilk, Bethany L. Ehlmann, Christopher S. Edwards, Kerri L. Donaldson Hanna, Valeriya Kachmar, Laura Lee, Jasper K. Miura, Carlé M. Pieters, Erin Pimentel, Katherine A. Shirley, David R. Thompson, Isabelle Adamczewski
Formal analysis: Angela M. Dapremont, Rachel L. Klima, Kierra A. Wilk
Funding acquisition: Rachel L. Klima, Bethany L. Ehlmann
Investigation: Angela M. Dapremont, Rachel L. Klima, Kierra A. Wilk, Bethany L. Ehlmann

© 2026. The Author(s).
This is an open access article under the terms of the Creative Commons Attribution License, which permits use, distribution and reproduction in any medium, provided the original work is properly cited.

1. Introduction

Spectroscopic data have provided a foundation for the identification and understanding of compositional characteristics of the lunar crust, including the distribution and abundance of major minerals and their chemistry. The full range of visible to near-infrared (VNIR) spectroscopy data, defined here as extending from ~0.3–5 μm (Bishop, 2019), acquired from orbital instrumentation and in situ studies of returned lunar samples have revealed the presence of the major rock forming silicate minerals olivine, pyroxene, and plagioclase feldspar (e.g., Adams & McCord, 1970; Kramer et al., 2011; Matsunaga et al., 2008). Opaque minerals (i.e., ilmenite, Mg-spinel) and amorphous materials (i.e., glass) have also been identified in lunar samples and spectrally on the Moon's surface (e.g., Adams et al., 1974; Pieters et al., 2011, 2019).

23335084, 2026, 3, Downloaded from https://agupubs.onlinelibrary.wiley.com/doi/10.1029/2025EA004557 by California Institute Of Tech, Wiley Online Library on [25/03/2026]. See the Terms and Conditions (https://onlinelibrary.wiley.com/terms-and-conditions) on Wiley Online Library for rules of use; OA articles are governed by the applicable Creative Commons License

Methodology: Angela M. Dapremont, Rachel L. Klima, Kierra A. Wilk, Bethany L. Ehlmann, Christopher S. Edwards, Kerri L. Donaldson Hanna, Valeriya Kachmar, Laura Lee, Jasper K. Miura, Carlé M. Pieters, Erin Pimentel, Katherine A. Shirley, David R. Thompson, Isabelle Adamczewski
Project administration: Bethany L. Ehlmann
Resources: Rachel L. Klima, Bethany L. Ehlmann, Kerri L. Donaldson Hanna, Jasper K. Miura, Isabelle Adamczewski
Software: Angela M. Dapremont, Kierra A. Wilk
Supervision: Rachel L. Klima, Bethany L. Ehlmann
Validation: Angela M. Dapremont, Rachel L. Klima, Kierra A. Wilk, Bethany L. Ehlmann
Writing – original draft: Angela M. Dapremont, Kierra A. Wilk, David R. Thompson
Writing – review & editing: Angela M. Dapremont, Rachel L. Klima, Kierra A. Wilk, Bethany L. Ehlmann, Christopher S. Edwards, Kerri L. Donaldson Hanna, Jasper K. Miura, David R. Thompson

The search for lunar water has primarily focused on the presence of the near infrared (near-IR) 3-μm absorption feature, which is indicative of hydroxyl (OH) and/or water (H_2O). In this region, OH exhibits its fundamental vibration at ∼2.7–2.8 μm and molecular H_2O exhibits its fundamental asymmetric and symmetric stretches between ∼2.8–2.9 μm, as well as its first bending overtone at ∼3.1 μm (Bishop et al., 1994; Clark et al., 1990). Early and geographically limited lunar orbital remote sensing data sets did not indicate the presence of hydration (OH/H_2O) on the lunar surface (e.g., Gillis & Lucey, 2004; Kieffer, 1995; Lucey et al., 2006). However, subsequent missions including the Moon Mineralogy Mapper (M^3) onboard the Chandrayaan-1 spacecraft, the Cassini Visual and Infrared Mapping Spectrometer (VIMS), the Deep Impact spacecraft infrared spectrometer, and the Chandrayaan-2 Imaging Infrared Spectrometer (IIRS) would later reveal the widespread presence of a broad and asymmetric 3-μm absorption feature consistent with hydration on the lunar surface (Chauhan et al., 2021; Clark, 2009; Pieters, Goswami, et al., 2009; Sunshine et al., 2009). M^3 observations have since been used to isolate potential indigenous lunar water/hydroxyl signatures in the central peak of Bullialdus Crater through coupling of geologic context and the identification of a 2.8-μm absorption feature attributed to OH bound to magmatic minerals excavated from depth (Klima et al., 2013), identify water signatures at lunar pyroclastic deposits (Li & Milliken, 2017; Milliken & Li, 2017), and support of the presence of exposed water ice at the north and south poles (Li et al., 2018). Resolving the speciation of lunar surface hydration, specifically OH versus H_2O, with some orbital remote sensing data sets has proven difficult; for example, M^3 does not exhibit the full 3-μm feature, 1.05–4.8 μm Deep Impact observations were spatially and temporally limited (Hampton et al., 2005), and Cassini VIMS observations were acquired over low spatial resolution (i.e., ∼175 km/pixel) (Clark, 2009). The Chandrayaan-2 IIRS, covering the 0.8–5.0 μm spectral range, has however, allowed for complete characterization of lunar hydration attributed to OH/H_2O presence (Chauhan et al., 2021). Lunar Trailblazer's High-resolution Volatiles and Minerals Mapper (HVM^3) was also designed to resolve the entire 3-μm feature, enabling a better understanding of the form, abundance, and distribution of water on the Moon.

Numerical indices, or parameters, are one useful way to quickly interpret and summarize spectroscopic features. The use of parameters for the analysis of VNIR spectroscopy data has proved successful at multiple Solar System mission destinations (e.g., Cheek et al., 2013; Pelkey et al., 2007; Staid et al., 2011; Viviano et al., 2014). The basis for the parameterization concept is that a single parameter value can capture a given spectral feature, with each individual parameter designed to capture a feature(s) unique to a specific mineralogy. Parameter values are calculated through the application of an algorithm, that uses combinations of spectral bands, to remotely sensed spectroscopic data sets. In addition to being qualitative indicators of location and relative abundance of minerals of interest, spectral parameters also serve as spatial distribution indicators since a parameter can be mapped across a region or globe to examine spatial variations of spectral features interpreted as associated mineralogy spatial variations (Pelkey et al., 2007).

The Lunar Trailblazer mission end was declared in July 2025 (Jet Propulsion Laboratory, 2025). Here, we detail the formulation and testing of spectral parameters in preparation for previously anticipated returned data from the Lunar Trailblazer HVM^3 science instrument (Ehlmann et al., this issue; Thompson et al., this issue). In this contribution, we use the visible to shortwave infrared (VSWIR) terminology in reference to the specific spectral range of HVM^3 (0.6–3.6 μm). Given the HVM^3 heritage from the M^3 imaging spectrometer, mineral parameter formulation and testing were conducted using M^3 data, and Deep Impact extended mission (EPOXI) data were used for water parameter testing. Despite prior existence of many of the presented parameters in M3Tools, through this contribution we seek to: demonstrate mineral parameter performance reliability through application to M^3 data of different spatial resolution, present a new OH/H_2O parameter for HVM^3, and provide a general VSWIR spectral parameter resource for the planetary science community. We first introduce the HVM^3, M^3, and Deep Impact instruments, followed by a presentation of the formulation and testing methodologies for both mineral- and water-related spectral parameters. We demonstrate parameter performance on both M^3 global image and Deep Impact/EPOXI lunar data sets, and conclude with an acknowledgment of parameter limitations.

2. Methods

2.1. Future and Current Data Sets

2.1.1. The High-Resolution Volatiles and Minerals Moon Mapper (HVM^3)

HVM^3 is one of two science instruments onboard Lunar Trailblazer (Ehlmann et al., this issue; Thompson et al., this issue; see Bowles et al., 2025 for Lunar Thermal Mapper (LTM) details). Lunar Trailblazer's primary

23335084, 2026, 3, Downloaded from https://agupubs.onlinelibrary.wiley.com/doi/10.1029/2025EA004557 by California Institute Of Tech, Wiley Online Library on [25/03/2026]. See the Terms and Conditions (https://onlinelibrary.wiley.com/terms-and-conditions) on Wiley Online Library for rules of use; OA articles are governed by the applicable Creative Commons License

science goal is to understand: (a) the abundance, distribution, and form of water on the Moon, and (b) the lunar water cycle. Trailblazer was also expected to collect data to benefit future lunar robotic and human exploration efforts through the Commercial Lunar Payload Services and Artemis programs, respectively.

Trailblazer has four science objectives: (a) detecting and mapping H_2O to determine its abundance, distribution, and form, (b) assessing lunar water time variation on sunlit surfaces, (c) mapping water ice in permanently shadowed regions, and (d) measuring surface temperature for local gradient quantification and searching for small cold traps.

HVM^3 would have acquired and delivered the highest spatial (50–90 m/pixel) and spectral (0.6 μm–3.6 μm; 10-nm spectral sampling) resolution VSWIR targeted data cubes of the Moon to date (Thompson et al., this issue)—an improvement upon the latitudinally limited (~60°N–30°S) M^3 data that were also acquired at 10 nm spectral sampling in targeted mode only (Boardman et al., 2011; Green et al., 2011). HVM^3 was designed to be able to distinguish various forms of identified lunar water and volatile species (OH, H2O, ice) with mineralogical context, thereby providing knowledge of lunar surface compositional characteristics including olivine, plagioclase, pyroxenes, and spinel group minerals. Through acquisition of VSWIR spectra out to 3.6 μm, HVM^3 would have also had the capability to resolve ambiguities in the exact position, shape, and strength of the 3-μm absorption feature and show the complete absorption features of OH, molecular water, and water ice (Bender et al., 2022).

The anticipated ≥1,000 targeted images acquired during Trailblazer's ≥1 year primary science phase was expected to provide ample data for spectral parameter construction and subsequent scientific analysis at a wide range of sites, including polar (e.g., permanently shadowed regions) and nonpolar regions, as well as locations of distinctive lithologic composition and latitudinal gradients of homogeneous composition (Ehlmann et al., this issue). Lunar Trailblazer was unique in the powerful instrument combination of coincident HVM^3 and LTM observations providing the best spectral discrimination, to date, of lunar minerals of interest. Furthermore, simultaneous temperature measurements at targeted lunar surface sites would have provided independent estimates of surface temperature to verify the thermal correction procedure applied to HVM^3 3-μm spectral region observations (Bowles et al., 2025).

2.1.2. The Moon Mineralogy Mapper (M^3)

The M^3 imaging spectrometer, launched in 2008 as a guest instrument onboard the Indian Space Research Organization's Chandrayaan-1 spacecraft, acquired data in two modes over the 0.46–2.976 μm wavelength range: global (140–280 m/pixel; 85 spectral channels; 20–40 nm spectral sampling) and targeted (70 m/pixel; 260 spectral channels; 10 nm spectral sampling) (Boardman et al., 2011; Green et al., 2011). Over two optical periods (OP), informally divided into segments OP1A, OP1B, OP2A, OP2B, and OP2C, >90% global coverage of the lunar surface was achieved by mission completion in 2009 (Boardman et al., 2011). M^3 provided the most complete near-IR spatial and temporal global scale coverage of the Moon to date, making these data the most appropriate for HVM^3 spectral parameter development and testing.

M^3 global spectral parameters have heritage from NASA's Clementine mission and the Mars Reconnaissance Orbiter Compact Reconnaissance Imaging Spectrometer for Mars. M^3 parameters were revised for hyperspectral data with a strong continuum slope and tested on lunar soil spectra of known compositions, as well as synthetic image cubes. M^3 parameters were made available to the scientific community via the M3Tools ENVI + IDL plugin for working with M^3 data (Nettles, 2020).

The library of M^3 global spectral parameter summary products includes pipeline, supplemental, and in-progress parameters. The M3Tools parameters classified as “pipeline” were those that were revised for hyperspectral data, while the parameters classified as “supplemental” were Clementine-derived or Clementine heritage parameters formulated for comparison with previous work. M^3 global wavelengths were used in parameter formulations. Pipeline mineral spectral parameter classes included: (a) reference I/F at various wavelengths, (b) band ratios, (c) continuum-removed band depths, (d) continuum-removed integrated band depths, and (e) absorption band minimum (i.e., center), full width half maximum (i.e., width), and symmetry; for example, at 1 μm. A visual representation, and brief description, of the commonly used band depth (i.e., absorption depth) and integrated band depth formulations is shown in Figure 1.

23335084, 2026, 3, Downloaded from https://agupubs.onlinelibrary.wiley.com/doi/10.1029/2025EA004557 by California Institute Of Tech, Wiley Online Library on [25/03/2026]. See the Terms and Conditions (https://onlinelibrary.wiley.com/terms-and-conditions) on Wiley Online Library for rules of use; OA articles are governed by the applicable Creative Commons License

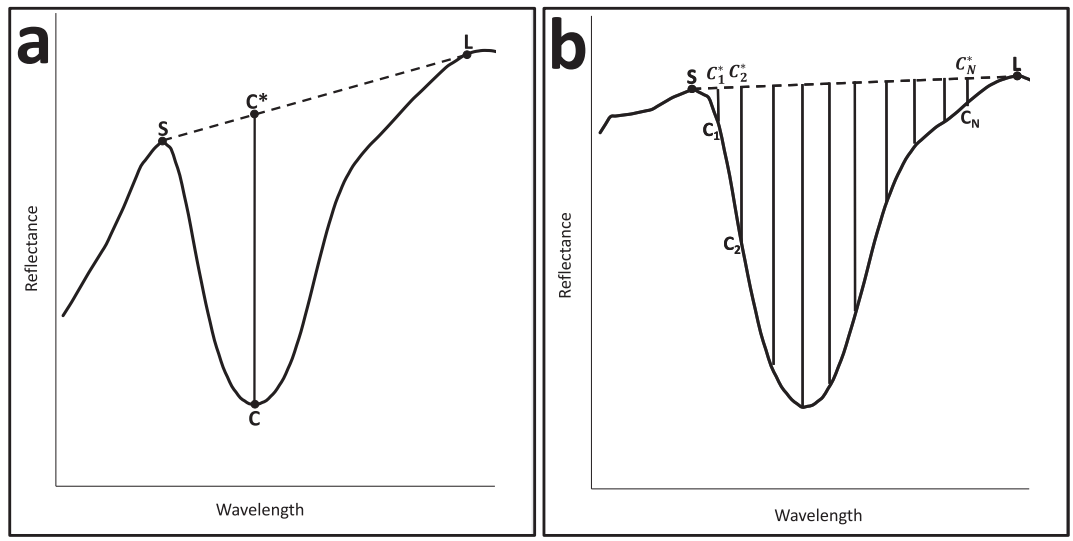


Figure 1. Visual representations of (a) band depth and (b) integrated band depth calculations. (a) Idealized spectrum with dashed line indicating continuum fit across absorption band. Band depth is calculated by $1 - R_c/R_{c*}$. At the absorption center point labeled C, R_c is the center wavelength (λ_c) reflectance. R_{c*} is the interpolated continuum reflectance, from the short (S) and long (L) wavelength points along the continuum, at the same wavelength. R_{c*} is equal to ($a*R_s + b*R_L$) with $a = 1 - b$ and $b = (\lambda_c - \lambda_s)/(\lambda_L - \lambda_s)$. (a, b) Are weighting parameters. (b) Idealized spectrum with dashed line indicating continuum fit across absorption band where short and long wavelength points are still used to define continuum but the continuum reflectance at a given wavelength (e.g., R_{c1*}) is used when summing band depths across the continuum.

Pipeline H_2O spectral parameters, discussed in further detail in Section 2.1.3, were also formulated with the intent of capturing near-IR OH spectral features, as well as 3-μm region H_2O and ice bands. The M^3 H_2O/OH indices did prove difficult to define and test however, due the lack of a sufficient "dry" lunar soil reference spectrum (i.e., all Reflectance Experiment LABoratory (RELAB) data were collected under purged air and not vacuum) (Tompkins & Pieters, 2010).

We also briefly describe here the M^3 thermal correction due to its relevance for accurate interpretation of lunar 3-μm region observations. The thermal correction approach of Clark et al. (2011) was applied to the M^3 reflectance data used for mineral parameter testing (i.e., NASA Planetary Data System Level 2). Known lunar and terrestrial material spectral properties were used to constrain greybody emission with an iterative approach used to project observed shorter wavelength reflectance properties to longer wavelengths. Thermal emission was taken as the positive difference between the observed and projected reflectance properties. Reflectance was estimated by deriving spectral emissivity and subtracting thermal emission from the observed spectrum with continued iterations until the derived thermal emission changed by less than 2 K, with a maximum of three iterations determined as the solution for lunar data. This approach has shown to provide sufficient accuracy to correct lunar reflectance spectra out to approximately 3.3 μm (Clark et al., 2011).

2.1.3. Deep Impact Extended Mission (EPOXI)

Since M^3 does not fully resolve the lunar 3-μm hydration feature, we conducted water-related parameter testing on data collected by the Deep Impact instrument calibration through its extended mission (EPOXI), using the High Resolution Instrument Infrared (HRI-IR) spectrometer. The Deep Impact spacecraft observed the Moon as a calibration body en route to the comet 103P/Hartley 2 flyby in November 2010 (Sunshine et al., 2009). We used spectra collected by the HRI-IR spectrometer on 5, 12, and 18 December 2009 (DOY 339, 346, and 352, respectively). These data were archived at the Planetary Data System Small Bodies Node (DIF-CAL-HRII-2-EPOXI-CALIBRATION S-V2.0, McLaughlin et al., 2011) and later calibrated by Laferriere et al. (2022). The Deep Impact/EPOXI data thermal correction is as follows.

We retrieved EPOXI surface reflectance and temperature simultaneously from radiance by applying a simple single-temperature emission model to instrument channels above 2,400 nm. We adopt a probabilistic formalism from model inversion theory (e.g., Rodgers, 2000; Tarantola, 2005). Our forward model $f(x)$ is a function of the

23335084, 2026, 3, Downloaded from https://agupubs.onlinelibrary.wiley.com/doi/10.1029/2025EA004557 by California Institute Of Tech, Wiley Online Library on [25/03/2026]. See the Terms and Conditions (https://onlinelibrary.wiley.com/terms-and-conditions) on Wiley Online Library for rules of use; OA articles are governed by the applicable Creative Commons License

retrieved surface state, which includes the vector-valued surface reflectance (ρ), the temperature (T), and a coefficient (α) which scales the surface-emitted signal to account for cold shadows:

$$f(x) = F_s\, \rho\, \pi - 1 + \alpha\, \epsilon\, L_\mathrm{e}(T)$$

Here F_s is the solar irradiance, is ϵ is the emissivity via Kirchhoff's law, $L_e(T)$ is the blackbody Planck emission at temperature T, in radiance units. The observed radiance L_o is the forward model perturbed by random instrument noise ψ_o:

$$L_o = f(x) + \psi_o$$

While this inversion can present as having more unknowns than measurements, we overcome this indeterminacy with a Bayesian prior over surface reflectance spectra (Thompson et al., 2018). We fit a multivariate Gaussian distribution (i.e., a multivariate normal distribution) in advance to RELAB library reflectances of lunar materials. This distribution has one dimension for each channel of spectral data. For each new EPOXI spectrum we condition this Gaussian on the observed channels below 2,400 nm, where no thermal emission is present. This conditional distribution serves as a prior over the reflectance for the channels greater than 2,400 nm. The most probable state (i.e., the Maximum A Posteriori solution) is that which minimizes the cost function:

$$\boldsymbol{\chi}^2(x) = (f(x) - L_o)^T\, S_{\boldsymbol{\epsilon}}^{-1}\, (f(x) - L_o) + (x - x_a)^T\, S_a^{-1}\, (x - x_a)$$

Where x_a is the prior mean, S_a is the prior covariance matrix, and $S_{\boldsymbol{\epsilon}}$ is the noise covariance matrix. The result is relatively insensitive to a selection of $S_{\boldsymbol{\epsilon}}$, but to promote close fitting of the measured EPOXI data, we provisionally set $S_{\boldsymbol{\epsilon}}$ to be diagonal with negligibly small noise values. We solve the above equation for reflectance and thermal state simultaneously by gradient descent. As noted in Thompson et al. (2018), regularization via diagonal loading of the prior covariance matrix is useful for numerical stability and to ensure the retrieved reflectance is free to fit arbitrary reflectance shapes.

3-μm region water-related parameters in the original M3Tools package included a 2.7-μm OH band depth (HBD2700), a 3-μm ice band depth (HBD2850) and a 3-μm H_2O band depth (BD3000). Additional infrared parameters included a 1.4-μm OH band depth (NBD1400), a 1.48-μm OH band depth (NBD1480), and a 2.3-μm OH band depth (NBD2300) (Nettles, 2020). The initial HVM^3 parameter pipeline will only include a 3-μm integrated band depth (IBD3000) parameter (Table 1) to capture lunar surface hydration presence as: (a) an update to the original M^3 spectral parameters package and (b) an improved method to embody the entire 3-μm OH/H_2O absorption feature of interest through a shift from a static band depth parameter to an IBD parameter.

Many of the Table 1 wavelength values are specific to M^3 data channels, with the indicated formulations intended to capture ideal continuum points and integrals (e.g., IBD parameters). The HVM^3 center wavelengths are slightly different. The package used to calculate the initial set of mineral spectral parameters discussed here will be made publicly available (see Data Availability Statement) at the time of publication thereby providing the scientific community with the opportunity to test potential improvement methods (e.g., the use of 10-nm step sizes on IBD parameters) for future orbital instrumentation at the Moon. Future work may result in minor shifts to parameter wavelengths to optimize performance and discrimination of investigated mineral or water phases. Our preparatory parameter testing was carried out using M^3 and Deep Impact/EPOXI data with a specific focus on verification of newly formulated parameters, necessary prior to HVM^3 arrival at the Moon.

We also note here the nomenclature used for unit referencing throughout this contribution; specifically, μm when referring to an instrument spectral range, as well as mineral and water reference spectra figure wavelength values (Figure 2; Figure 9), and nm when referring to instrument spectral sampling and acquired spectra figure wavelength values (Figures 4–8; Figure 10).

2.2. Mineral Parameters

In an effort to capture the full mineralogical diversity of the Moon revealed by M^3, we added several newly updated mineral parameters to the existing M^3 global spectral parameter summary products library. These newly added parameters were subsequently tested for efficacy, individually and along with existing M^3 spectral

Earth and Space Science

10.1029/2025EA004557

Table 1
Mineral and Water Spectral Parameters That Were Developed and Tested Using M^3 and Deep Impact/EPOXI Lunar Data Sets

Name	Parameter	Formulation	Rationale	M3 original?	Parameter type
R1580	1.6 μm reflectance	reflectance at 1,579 nm	IR albedo	YES	mineral
IBD1000	1 μm integrated band depth	integrated band depth over 1,000 nm spectral region with 1 μm continuum reflectance at the given wavelength (sums band depths from 789 to 1,308 nm)	Fe mineralogy (e.g., pyroxenes, olivines, glasses)	YES	mineral
IBD2000	2 μm integrated band depth	integrated band depth over 2,000 nm spectral region with 2 μm continuum reflectance at the given wavelength (sums band depths from 1658 to 2,498 nm)	Fe mineralogy (e.g., pyroxenes, glasses, spinels)	YES	mineral
1 μm_Min	1 μm band center	wavelength between 890 and 1,349 nm at which band depth is maximized	Fe mineralogy	YES	mineral
BD1900	band depth at 1.9 μm: low Ca pyroxene index	1-((R1898)/((R2498-R1408/2498-1408)*(1898-1408) + R1408))	Pyroxene will be positive; favors LCP	YES	mineral
BD2300	band depth at 2.3 μm: high Ca pyroxene index	1-((R2298)/((R2578-R1578/2578-1578)*(2298-1578) + R1578))	Pyroxene will be positive; favors HCP	YES	mineral
IBD1250	1.25 μm spectral region integrated band depth	integrated band depth over the 1,250 nm spectral region with 1.25 μm continuum reflectance at the given wavelength (sums band depths from 1029 to 1698 nm)	Fe-bearing Plagioclase	NO	mineral
BD1250	1.25 μm band depth	1-((R1249)/((R1579-R749/1579-749)*(1249-749) + R749))	Plagioclase comparison with Kaguya	YES	mineral
OLINDEX	M3 olivine index	0.1((R1750-R650/1750-650)*(860-650) + R650)/R860)+0.5((R1750-R650/1750-650)*(1047-650)+(R650))/(R1047)+0.25((R1750-R650/1750-650)*(1230-650) + R650)/(R1230)	Olivine	YES	mineral
R1400_1750	Mg-spinel indicator	(R1409 + R1429)/(R1739 + R1778)	Mg-spinel	NO	mineral
IBD3000	3 μm integrated band depth	integrated band depth over 3,000 nm spectral region (straight line continuum fit between 2.6 and 3.6 μm)	OH/H2O	NO	water

23335084, 2026, 3, Downloaded from https://agupubs.onlinelibrary.wiley.com/doi/10.1029/2025EA004557 by California Institute Of Tech, Wiley Online Library on [25/03/2026]. See the Terms and Conditions (https://onlinelibrary.wiley.com/terms-and-conditions) on Wiley Online Library for rules of use; OA articles are governed by the applicable Creative Commons License

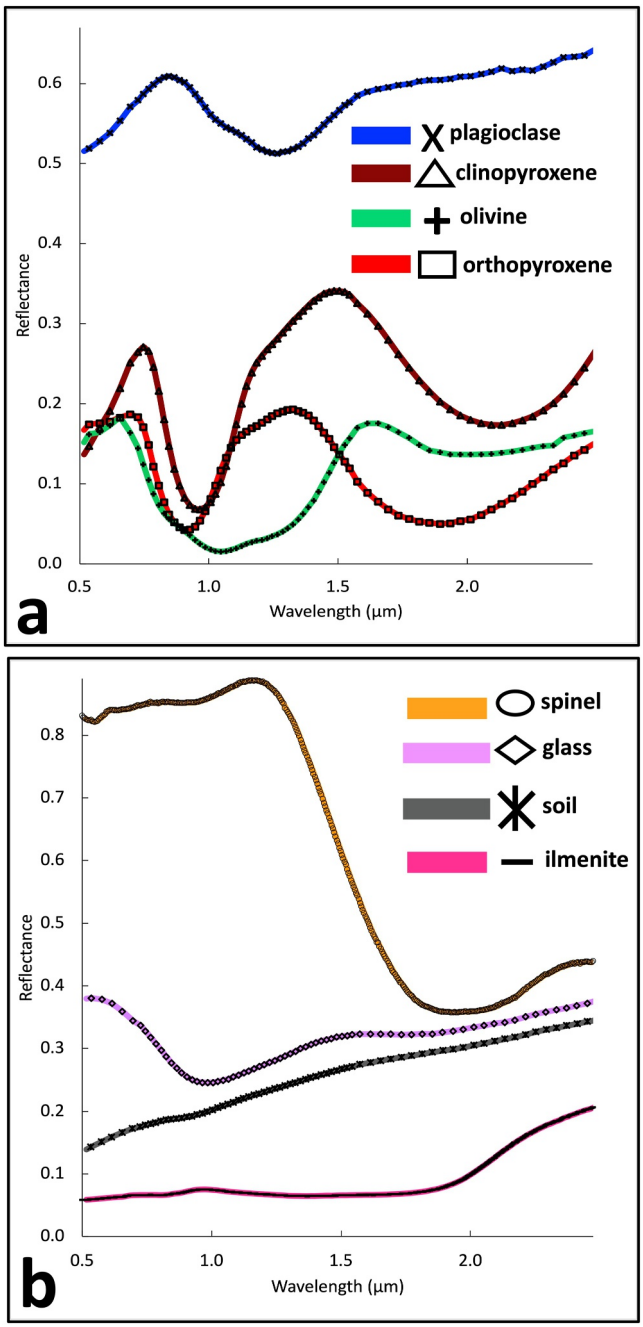


Figure 2. Lunar mineral VSWIR spectra. Solid lines are M3Tools and RELAB reference spectra convolved to HVM^3 bandpasses. Symbols overtop solid lines are M3Tools and RELAB reference spectra. Well-correlated laboratory and convolved spectra support confidence that HVM^3 and derived reflectance products would have captured lunar mineralogical diversity well. (a) Blue spectrum is plagioclase (plagioclase_15415_0-500), dark red spectrum is clinopyroxene (clinopyroxene_12063_0-45), bright red spectrum is orthopyroxene (orthopyroxene_78235_0-250), and green spectrum is olivine (olivine_72415_Bulk). (b) Orange spectrum is spinel (specimen ID: SP-CMP-127-B), lavender spectrum is glass (maskelynite_A881757_94-200), gray spectrum is lunar soil (avg62231_global soil), and pink spectrum is ilmenite (specimen ID: LR-CMP-182). Plot legends denote mineral names that correlate with spectra colors and symbols.

parameters, using M^3 global data (i.e., the M^3 global wavelengths used). In summary, our testing objectives were to: formulate new parameters not included in the original M3Tools package (e.g., IBD1250, R1400_1750), assess newly developed parameter performance independently and with existing "legacy" M^3 parameters, and use M^3 global data (i.e., mosaics and individual strips) to determine initial quantitative detection thresholds for robust mineral identification. Although some of the parameters tested here, such as IBD1000 and IBD2000, are well-established metrics for identifying ferrous minerals (e.g., pyroxene, olivine), the M3Tools spectral parameters have never, to the best of our knowledge, been reported on all together in a single peer-reviewed publication. Therefore, this contribution is intended to serve as a centralized resource for the scientific community that includes an assessment of both existing and updated parameters widely used in the literature as those anticipated for the interpretation of Lunar Trailblazer parameter map data products, and for planned lunar composition investigations from orbit (e.g., Blue Origin, 2025; Firefly Aerospace, 2025).

Table 1 details the new and existing parameters based on M^3 spectral parameter formulations. Parameter testing was conducted using M^3 global image cubes (140–280 m/pixel) at known locations of well characterized mineralogical diversity on the lunar surface (e.g., Aristarchus crater, Proclus crater) (Donaldson Hanna et al., 2014; Mustard et al., 2011), as well as the M^3 OP2C1 spatially binned (~1.4 km/pixel) simple cylindrical global mosaic since this latter data set provided the largest spatial coverage of the Moon (Besse et al., 2013). The global mosaic was also used to determine quantitative thresholds for individual parameters, examples of which are shown in this contribution. More specifically, an initial range of quantitative detection threshold values using mineral indicator parameter map (e.g., olivine OLINDEX parameter, plagioclase IBD1250 parameter) lunar lithology identifications were narrowed until a range deemed sufficiently representative of a mineral of interest was determined. Threshold values are intended to represent robust detections for specific lunar minerals of interest (Pelkey et al., 2007). We acknowledge that the presented threshold values may be revised and improved upon specifically for future orbital lunar instrumentation.

3. Results

3.1. Mineral Parameters

Mineral parameters are organized and described below by parameter name. We do this, in part, to caution against misinterpretations of lunar mineralogy based solely on spectral parameters upon delivery to the scientific community. We also stress the importance of validating mineral signatures as indicated by spectral parameters with VSWIR reflectance spectra (Figure 2).

3.1.1. IBD1000 & IBD2000

The 1-μm integrated band depth (IBD1000) and 2-μm integrated band depth (IBD2000) M^3 spectral parameters continue to perform well singly and in concert in capturing Fe^{2+} mineralogy when applied to the M^3 OP2C1 global mosaic used for parameter testing (Figure 3), as well as M^3 global image cubes tested with newly developed parameters (Figures 4–8). The "standard" M^3 RGB color composite in Figure 3 demonstrates how the IBD1000 and IBD2000 spectral parameters can differentiate between the dark, smooth mare basalts and the high albedo highlands that comprise the lunar dichotomy.

23335084, 2026, 3, Downloaded from https://agupubs.onlinelibrary.wiley.com/doi/10.1029/2025EA004557 by California Institute Of Tech, Wiley Online Library on [25/03/2026]. See the Terms and Conditions (https://onlinelibrary.wiley.com/terms-and-conditions) on Wiley Online Library for rules of use; OA articles are governed by the applicable Creative Commons License

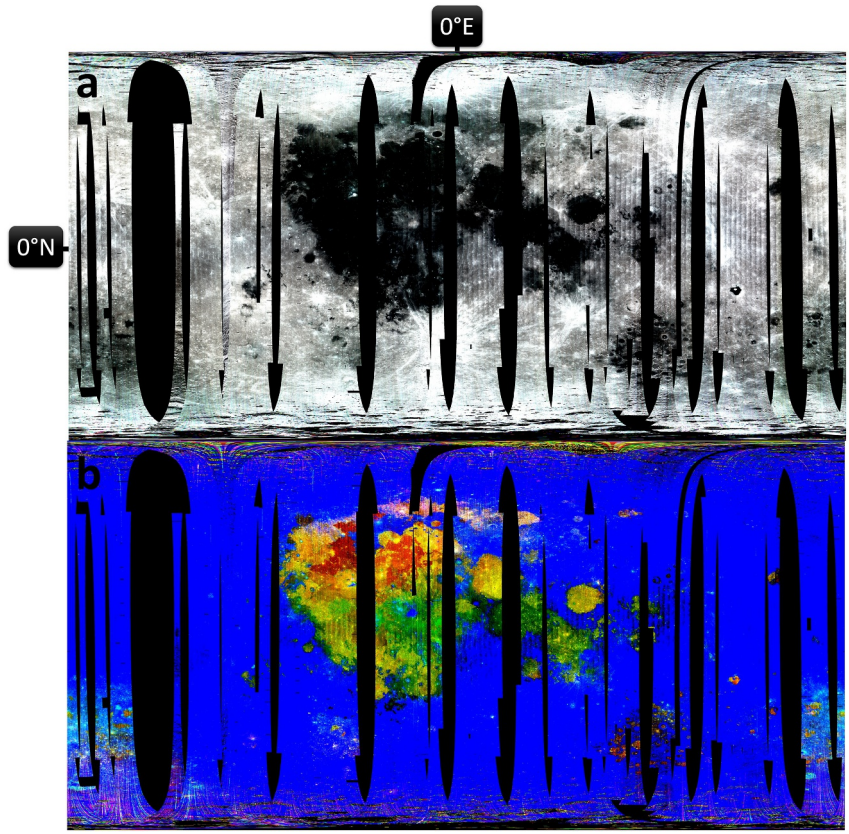


Figure 3. (a) M^3 OP2C1 spatially binned (~1.4 km/pixel) simple cylindrical projection global mosaic, centered at 0° longitude, showing lunar maria and highlands materials distribution. (b) R:IBD1000 G:IBD2000 B: R1580 "standard" M^3 color composite showing mare and highland mineralogy differences, as well as compositional diversity within the maria, as revealed by IBD1000 and IBD2000 spectral parameters (i.e., red color indicating olivine presence, yellow indicating pyroxene presence and, blue denoting highland materials). North is up in this mosaic image and all subsequent M^3 images.

Parameters also reveal mineralogical diversity within the mare specifically, regions of olivine- and pyroxene-rich materials (e.g., Figure 5f). While these IBD parameters are not intended to reveal specific absorption band positions at 1 and 2 μm, we demonstrate that they do succeed at their intended purpose of capturing pyroxene presence with a range of compositional diversity on the Moon. More specifically, for each type of pyroxene, the IBD1000 parameter and IBD2000 parameter individually can indicate this mineral's presence (i.e., identify pyroxene regardless of composition). Used together these parameters can also aid in differentiating lunar surface regions with pyroxenes (i.e., discriminate pyroxenes of different composition with limitations on exactly how they are different) and Fe-bearing glasses (both IBD1000, IBD2000), as well as olivines (IBD1000 only) and spinels (IBD2000 only) present along with the acquisition of VSWIR spectra.

Pyroxene spectra are characterized by broad diagnostic absorptions near 1 and 2 μm (Figure 2) caused by crystal field transitions of Fe in octahedral coordination (Burns, 1993). Orthopyroxenes ($(Fe, Mg)_2Si_2O_6$) and clinopyroxenes ($(Ca, Fe, Mg)_2Si_2O_6$) both have two octahedral cation sites, M1 and M2, with Fe^{2+} electronic transitions in the M2 site producing the strongest absorptions near 1 and 2 μm. The 1 and 2 μm absorption positions shift to longer wavelengths within increasing Fe^{2+} and Ca^{2+}, generally, and since Ca^{2+} is low for orthopyroxenes, band positions reflect the Mg^{2+}/Fe^{2+} ratio differences; thus, the highest-Mg and lowest-Ca pyroxenes exhibit the shortest 1 and 2 μm absorption band positions (Klima et al., 2011).

3.1.2. OLINDEX

The original M^3 olivine index spectral parameter (OLINDEX) is intended to reveal strong positive parameter values through detection of the broad olivine absorption centered near 1 μm, similar to the rationale of other nonlunar OLINDEX parameters (Pelkey et al., 2007; Viviano et al., 2014). The OLINDEX parameter performed well

23335084, 2026, 3, Downloaded from https://agupubs.onlinelibrary.wiley.com/doi/10.1029/2025EA004557 by California Institute Of Tech, Wiley Online Library on [25/03/2026]. See the Terms and Conditions (https://onlinelibrary.wiley.com/terms-and-conditions) on Wiley Online Library for rules of use; OA articles are governed by the applicable Creative Commons License

10.1029/2025EA004557

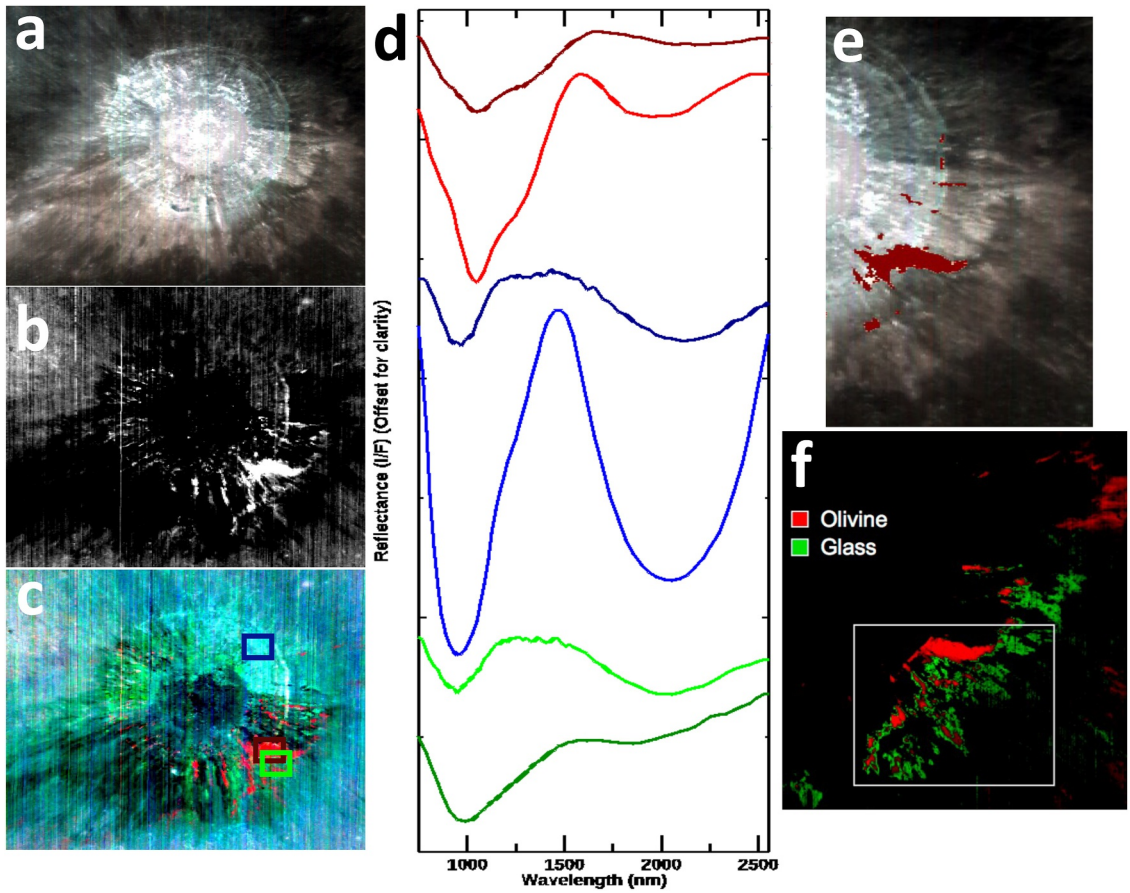


Figure 4. Aristarchus crater spectral parameter testing. (a) M^3 image M3G20090612t060502 (OP2C1) of Aristarchus crater (~40 km diameter). (b) M^3 OLINDEX parameter in greyscale. (c) R:OLINDEX G:IBD2000 B:BD2300 parameter color composite. (b, c) OLINDEX parameter with the following threshold applied: 0.861–0.927. (d) Spectral plot with M^3 spectra acquired from (a), along with reference spectra, consistent with olivine and pyroxene presence at Aristarchus crater. Spectra from top to bottom are as follows: M^3 spectrum from location denoted by dark red box overtop (c) (4.525605, 47.911500), olivine_72415_0-45 reference spectrum, M^3 spectrum from location denoted by dark blue box overtop (c) (4.525633, −47.911504), pyroxene_A881757_200-370 reference spectrum, M^3 spectrum from location denoted by lime green box overtop (c), maskelynite_A881757_94-200 reference spectrum. All spectra in this figure and subsequent mineral spectral parameter figures (i.e., Figures 5–8) are continuum removed to enhance absorption features of interest. (e) Subset of (a) with OLINDEX threshold parameter results overlain. (f) Aristarchus crater olivine (red) and glass (green) distribution at the same area as (e) using the Spectral Angle Mapper (SAM) algorithm of Mustard et al. (2011). Figure modified from Mustard et al. (2011). Note similar results among OLINDEX parameter and Mustard et al. (2011) SAM algorithm. M^3 spectrum acquired from Mustard et al. (2011) SAM algorithm glass detection location and maskelynite reference spectrum included for context.

at the Aristarchus test site when compared with other previously documented spectral mapping methods (Figure 4), and on the M^3 global mosaic (Figure 5).

Lunar olivine identifications extend back to telescopic measurements of the Moon (Pieters et al., 1980; Staid & Pieters, 2001). Subsequent analysis revealed olivine-rich material and olivine as a common component in returned highland samples and some Apollo basalts, respectively (e.g., Heiken et al., 1991). M^3 confirmed the presence of olivine in Ti-rich mare basalts (Staid et al., 2011), and olivine identifications extend across the Moon in the lunar highlands, around basin exposures (Yamamoto et al., 2010), and locally co-existing with other lithologies (e.g., Kramer et al., 2013); for example, at crater central peaks and walls.

The broad olivine ($(Mg, Fe)_2SiO_4$) absorption near 1 μm is the result of Fe^{2+} electronic transitions in three cation sites within the mineral's crystal structure resulting in overlapping spectral features (Burns, 1993) (Figure 2). The OLINDEX parameter tested here is intended to capture the relative strengths of the triplet features that comprise the broad olivine absorption in an effort to distinguish these component absorption features. Interestingly, more recent work has demonstrated relevance of an asymmetric Gaussian to fit four overlapping bands to the characteristic 1 μm olivine absorption feature (Brown, 2025). In their analysis of lunar olivine-rich lithologies, Isaacson et al. (2011) highlighted olivine-rich areas using an IBD ratio of the band strengths at 1 and 2 μm. In their

23335084, 2026, 3, Downloaded from https://agupubs.onlinelibrary.wiley.com/doi/10.1029/2025EA004557 by California Institute Of Tech, Wiley Online Library on [25/03/2026]. See the Terms and Conditions (https://onlinelibrary.wiley.com/terms-and-conditions) on Wiley Online Library for rules of use; OA articles are governed by the applicable Creative Commons License

10.1029/2025EA004557

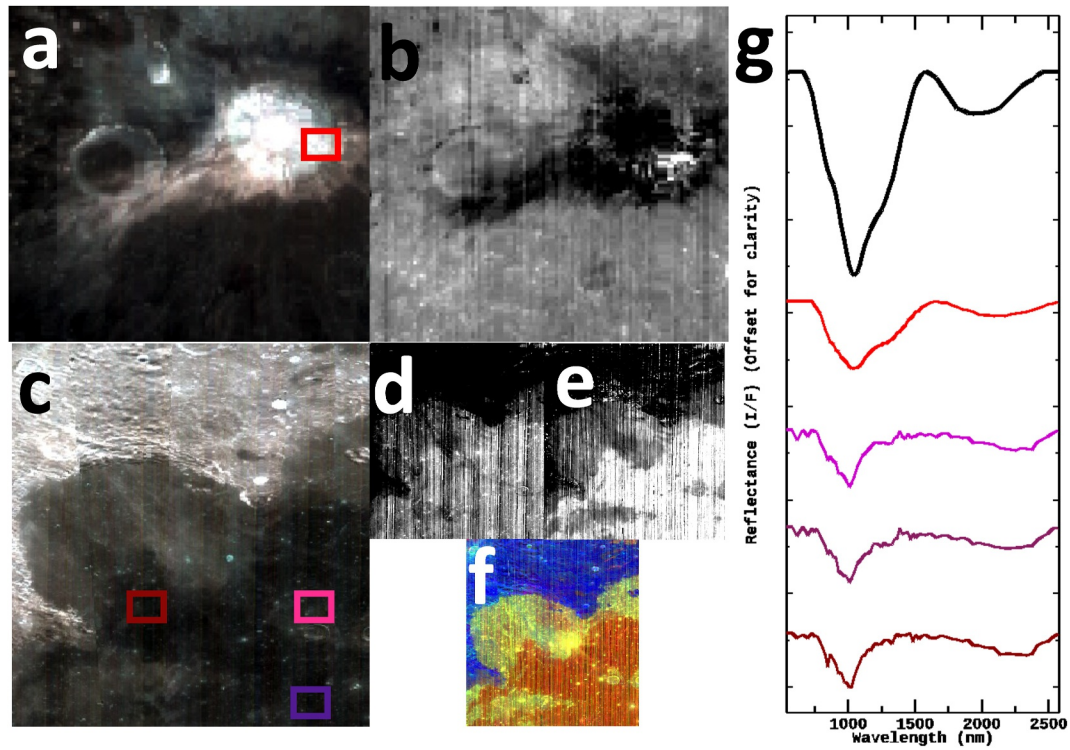


Figure 5. OLINDEX global mosaic spectral parameter testing. (a) M^3 global mosaic image (OP2C1) of Aristarchus crater (~40 km diameter). (b) Image (a) OLINDEX parameter with the following threshold applied: 0.840–0.927. (c) M^3 global mosaic image (OP2C1) of Sinus Iridum region. Image is ~1,200 km across. (d) Image (c) OLINDEX parameter with the following threshold applied: 0.840–0.927. (e) Image (c) IBD1000/IBD2000 parameter ratio. (f) Image (c) in R:IBD1000 G: IBD2000 B:R1580 parameter color composite. (g) Spectral plot with M^3 spectra acquired from (a, c), along with reference spectra, consistent with olivine spectral signatures. Spectra from top to bottom are as follows: olivine_72415_0-45 reference spectrum, M^3 spectrum from location denoted by red box overtop (a) (23.429084, −46.904334), M^3 spectra from locations denoted by color boxes overtop (c) (5 × 5 averages). Spectra colors correlate with box colors.

1 μm/2 μm ratio formulation, spectra with strong 1 μm features and weak 2 μm features would have high values. This simple band ratio parameterization was shown to be useful when compared with our M^3 OLINDEX parameter testing results (Figure 5e) and may therefore, be valuable for future orbital VSWIR spectrometers at the Moon.

3.1.3. IBD1250

The BD1250 M^3 spectral parameter was designed to identify the presence of crystalline plagioclase ((Ca,Na)(Al, $Si)_4O_8$)) using the band depth near 1,250 nm. The diagnostic 1,250 nm plagioclase absorption feature was identified in both Selenological and Engineering Explorer (SELENE)/Kaguya Multiband Imager data (Ohtake et al., 2009) and M^3 data, following a lack of definitive spectral evidence for anorthosite from both Earth-based telescopic and remotely sensed data of the Moon (e.g., Hawke et al., 2003). Relative to this M^3 heritage parameter, we updated the HVM^3 spectral library to include an integrated band depth parameter for plagioclase detection (IBD1250) based on the formulation of Cheek et al. (2013) who identified and conducted a detailed study of crystalline anorthosite, a rock composed of >90 wt. % plagioclase, at the Orientale basin. This formulation was also later used to globally map crystalline plagioclase (Donaldson Hanna et al., 2014). We demonstrate that our updated IBD1250 parameter can be used successfully, alone and in RGB color composite, for crystalline plagioclase identification (Figures 6c–6e).

The diagnostic crystal field absorption of plagioclase near 1,250 nm is caused by electronic transitions in Fe^{2+} cations which substitute for Ca^{2+} in an irregular 8- to 12-fold site (e.g., Adams & Goullaud, 1978; Bell & Mao, 1973). The Moon's primary anorthositic crust (i.e., the lunar highlands) is dominated by plagioclase (Pieters et al., 2019), with crystalline plagioclase mapped across the Moon by multiple orbital remote sensing instruments

23335084, 2026, 3, Downloaded from https://agupubs.onlinelibrary.wiley.com/doi/10.1029/2025EA004557 by California Institute Of Tech, Wiley Online Library on [25/03/2026]. See the Terms and Conditions (https://onlinelibrary.wiley.com/terms-and-conditions) on Wiley Online Library for rules of use; OA articles are governed by the applicable Creative Commons License

10.1029/2025EA004557

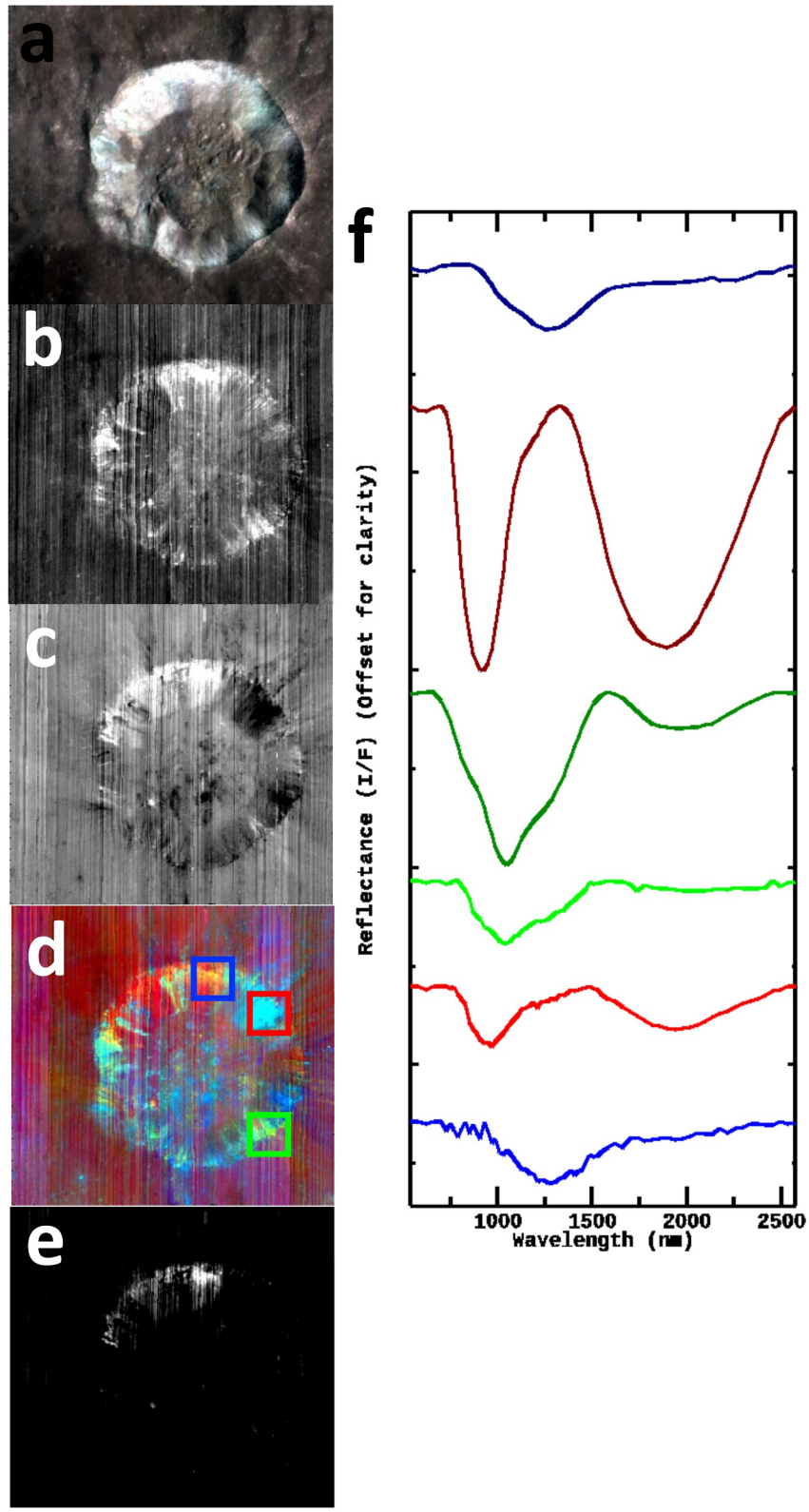


Figure 6.

23335084, 2026, 3, Downloaded from https://agupubs.onlinelibrary.wiley.com/doi/10.1029/2025EA004557 by California Institute Of Tech, Wiley Online Library on [25/03/2026]. See the Terms and Conditions (https://onlinelibrary.wiley.com/terms-and-conditions) on Wiley Online Library for rules of use; OA articles are governed by the applicable Creative Commons License

23335084, 2026, 3, Downloaded from https://agupubs.onlinelibrary.wiley.com/doi/10.1029/2025EA004557 by California Institute Of Tech, Wiley Online Library on [25/03/2026]. See the Terms and Conditions (https://onlinelibrary.wiley.com/terms-and-conditions) on Wiley Online Library for rules of use; OA articles are governed by the applicable Creative Commons License

(Donaldson Hanna et al., 2014; Ohtake et al., 2009; Pieters, Boardman, et al., 2009). We acknowledge that there are plagioclase detection difficulties in the form of the presence of "featureless" plagioclase characterized by a spectrum with no absorption features near 1, 1.25, and 2 μm, and often observed contiguously with lunar highlands "pure" anorthosites which likely lack Fe in their crystal structure (Ohtake et al., 2009). However, our integrated band depth plagioclase parameter is designed to detect the 1.25 μm due to crystalline Fe-bearing plagioclase on the Moon.

3.1.4. R1400_1750

Mg-spinel ($MgAl_2O_4$), initially detected by M^3 on the lunar farside at Moscoviense Basin, is spectrally characterized by the lack of a 1-μm ferrous absorption with a prominent and broad absorption near 2 μm (Pieters et al., 2011). Mg-spinel identifications have since extended across the lunar highlands crust, and to several basin geologic settings (Pieters et al., 2014; Sodha & Dhingra, 2025; Sun et al., 2017). Spinels exhibit a strong electronic transition absorption near 2 μm due to different amounts of Fe^{2+} in a tetrahedral site (Cloutis et al., 2004).

Pieters et al. (2014) presented a spinel ratio (R1400/R1750), to approximate Mg-spinel band strength variations, that we have added to the M^3 spectral library and subsequently tested at the Moscoviense detection site, as well as globally. While this new ratio parameter could be used locally to distinguish Mg-spinel detections in an RGB color composite at Moscoviense (Figure 7), the ability to differentiate spinel and pyroxene globally was more challenging (Figure 8). We note that a strong IBD2000 and a weak IBD1000 could also be a characteristic combination of parameters to aid in spinel detection.

3.2. Water Parameters

The IBD3000 integrated band depth parameter presented here is intended to be used as a lunar surface hydration signature indicator by providing a measure of the total strength of the hydration feature between 2.6–3.6 μm. This 3-μm absorption feature can be attributed to the presence of OH (fundamental vibration between ∼2.7–2.8 μm) and/or H_2O (asymmetric and stretches between ∼2.8 and 2.9 μm with first bending overtone at ∼3.1 μm) (Bishop et al., 1994; Clark et al., 1990) (Figure 9). The lunar 3-μm hydration feature is characterized by an absorption minimum near ∼2.8 μm that increases in reflectance asymmetrically toward longer wavelengths (Sunshine et al., 2009). Figure 10 is an example of the consistent 3.0-μm absorption feature that we observe across the surface of the lunar southern hemisphere upon application of this parameter to Deep Impact/EPOXI data, supporting the parameter reliability for HVM^3. It is also apparent from Figure 10b that variations in the strength of the 3-μm feature exist across the lunar surface. This observation correlates with prior work (e.g., Laferriere et al., 2022) that documented variations in the strength of hydration signatures at the southern hemisphere of the Moon and concluded that they were largely dependent on instantaneous temperature and composition. Additional factors that could influence these observed variations include latitude and time of day. A detailed assessment of the 3-μm feature strength differences is beyond the scope of this manuscript intended to focus on the methodology and application of a new reliable water parameter for the Moon. For further detail on the variations in the 3-μm feature in the data set from which Figure 10 is derived, we refer the reader to Laferriere et al. (2022).

Deep Impact/EPOXI spectra acquired during IBD3000 spectral parameter testing does reveal similarities with IIRS Level-2 photometrically corrected reflectance image data. IIRS reflectance spectra acquired from Mare Nubium basin (Chauhan et al., 2025 Figure 8bi) and close to Malapert A crater at the lunar south polar region (Chauhan et al., 2025 Figure 10bi) exhibit absorption features of similar shape and position near ∼2.8 μm as those from the southern hemisphere of the Moon revealed by Deep Impact/EPOXI (Figure 10c). The consistency of these results, as well as the comparable spectral coverage (Chauhan et al., 2021; Hampton et al., 2005) among

Figure 6. Proclus crater spectral parameter testing. (a) M^3 image M3G20090202T024131 (OP1B) of Proclus crater (∼27 km diameter). (b) M^3 BD1250 parameter in greyscale. (c) M^3 IBD1250 parameter in greyscale. (d) R: IBD1250 G: IBD1000 B: IBD2000 parameter color composite. (e) Image (c) with the following threshold applied: 0–1.37. (f) Spectral plot with M^3 spectra acquired from (a) consistent with plagioclase, pyroxene, and olivine presence at Proclus crater. Spectra from top to bottom are as follows: plagioclase_15415_0-500 reference spectrum, orthopyroxene_78235_0-250 reference spectrum, olivine 72415_0-45 reference spectrum, M^3 spectrum from location denoted by green box overtop (d) (15.827594, 47.204937), M^3 spectrum from location denoted by red box overtop (d) (16.307904, 47.220360), M^3 spectrum from location denoted by blue box overtop (d) (16.479159, 46.955823).

10.1029/2025EA004557

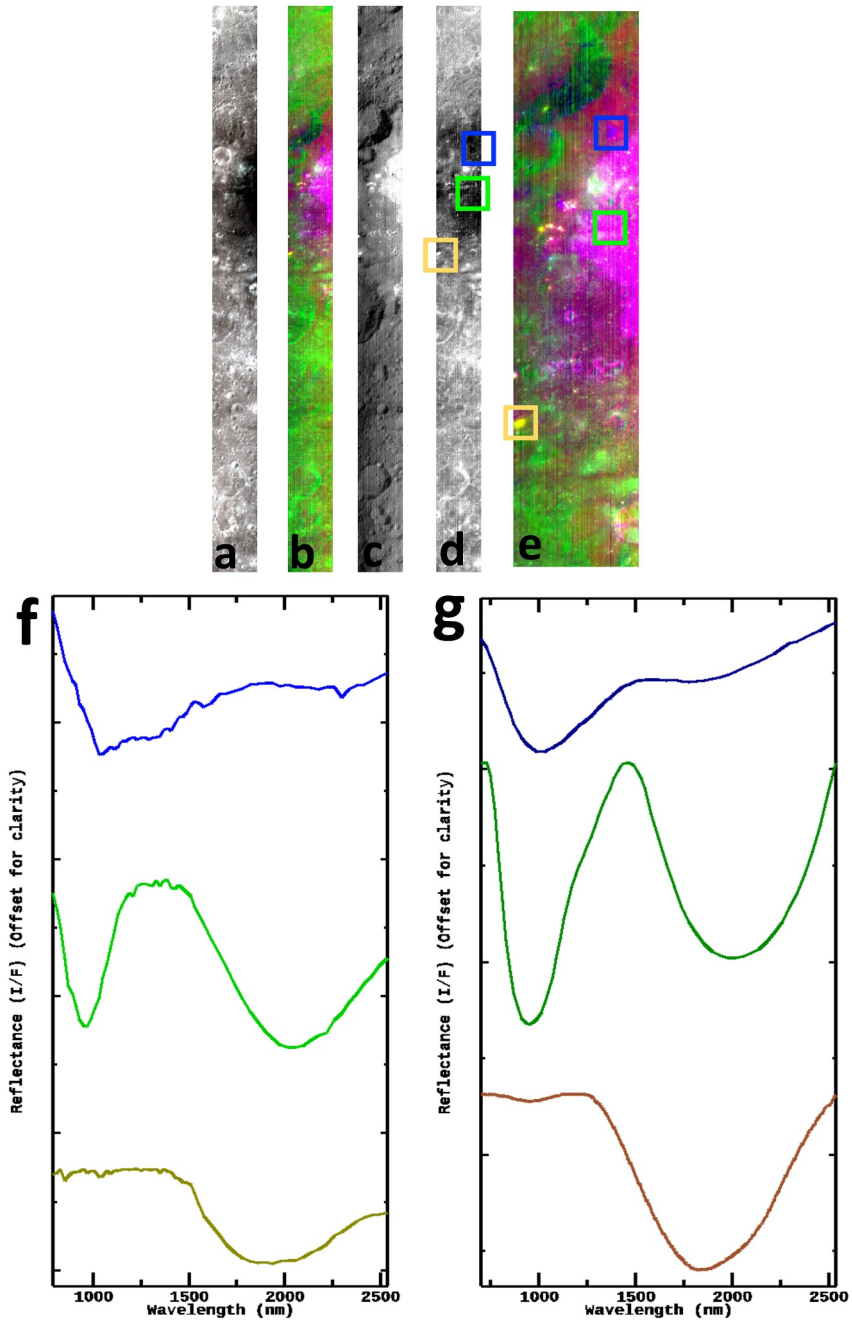


Figure 7. Moscoviense spectral parameter testing. (a) M^3 image M3G20090125T172601 (OP1B) of original Mg-spinel detection (Pieters et al., 2011). (b) R: IBD2000 G: R1440_R1750 B: IBD1000 parameter color composite of image (a). (c) Image (a) IBD2000 parameter in greyscale. (d) Image (a) R1440_R1750 parameter in greyscale. (e) Close-up view of image (b) color composite. (f) Spectral plot with M^3 spectra acquired from sites denoted by color boxes overtop (d) and (e). Spectra colors correspond with box colors. (g) Spectral plot with reference spectra from top to bottom as follows: maskelynite_A881757_gt370, pyroxene_A881757_gt370, specimen ID: SP-CMP-127-B.

instrument data, suggests that the presented IBD3000 parameter formulation would likely perform reliably when applied to high-resolution IIRS data—an opportunity space for future work particularly when radiometric calibration of IIRS data beyond 3.5 μm has been finalized (Chauhan et al., 2025).

23335084, 2026, 3, Downloaded from https://agupubs.onlinelibrary.wiley.com/doi/10.1029/2025EA004557 by California Institute Of Tech, Wiley Online Library on [25/03/2026]. See the Terms and Conditions (https://onlinelibrary.wiley.com/terms-and-conditions) on Wiley Online Library for rules of use; OA articles are governed by the applicable Creative Commons License

10.1029/2025EA004557

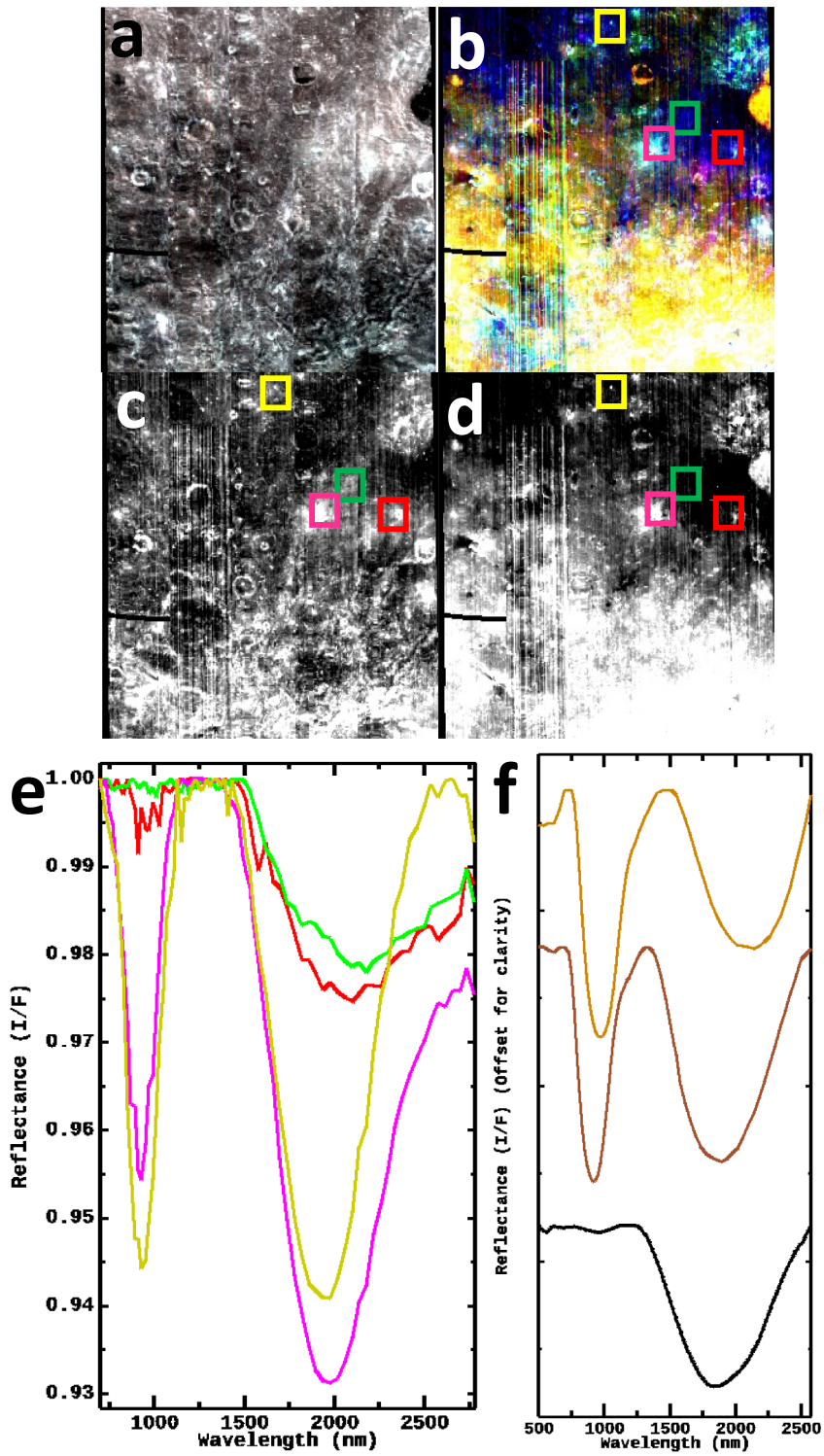


Figure 8. R1440_R1750 Mg-spinel indicator global mosaic spectral parameter testing. (a) M^3 global mosaic image (OP2C1) of Zwicky test site. Image is ∼1,200 km across. (b) Image (a) R:IBD1000 G:IBD2000 B: R1440_R1750 parameter color composite. (c) Image (a) R1440_R1750 parameter in greyscale. (d) Image (a) IBD2000 parameter in greyscale. (e) Spectral plot of M^3 spectra acquired from locations denoted by color boxes overtop (b–d) consistent with pyroxene and Mg-spinel presence at Zwicky test site. Green spectrum (−17.566043, 169.104899), red spectrum (−18.674019, 170.628366), yellow spectrum (−13.918954, 166.242626), and magenta spectrum (−18.535522, 167.950757) correspond to color boxes overtop (b–d). (f) Spectral plot of reference spectra from top to bottom as follows: clinopyroxene_12063_0-250, orthopyroxene_78235_0-250, specimen ID: SP-CMP-127-B.

23335084, 2026, 3, Downloaded from https://agupubs.onlinelibrary.wiley.com/doi/10.1029/2025EA004557 by California Institute Of Tech, Wiley Online Library on [25/03/2026]. See the Terms and Conditions (https://onlinelibrary.wiley.com/terms-and-conditions) on Wiley Online Library for rules of use; OA articles are governed by the applicable Creative Commons License

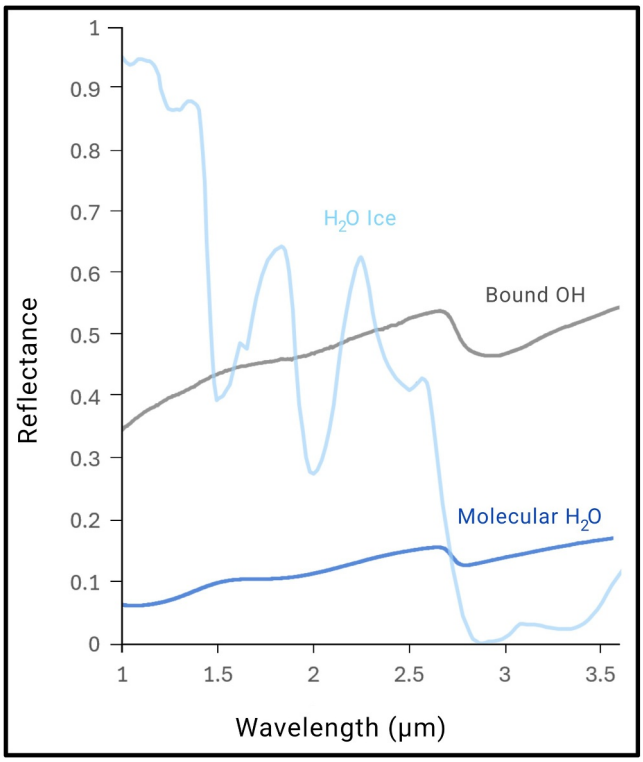


Figure 9. Reference spectra plot showing spectral signatures of the different forms of water (OH, H_2O, ice) to be investigated by Lunar Trailblazer (Ehlmann et al., 2022). Bound OH spectrum is RELAB specimen ID: BE-JFM-061. H_2O ice spectrum is 100% water ice (Calvin & Clark, 1991). Molecular H_2O spectrum is Apollo 17 soil sample, RELAB database BKR1LR117. Contamination from organics in the optical path near 3.3–3.4 μm was spliced and replaced by linear interpolation.

3.3. Parameter Limitations

Interpretations about mineral presence made from spectral parameters can be influenced by many of the same factors that complicate the VSWIR reflectance spectra from which they are derived including, material particle size, surface texture, and mineral mixtures, among others (e.g., Clark, 1999; Hapke, 1993). Given that it is typical to encounter mineral mixtures on the surfaces of terrestrial bodies in the Solar System, we acknowledge that the spectral parameters presented here, intended as a guide for the presence of a particular spectral feature, may not always be exclusive to one type of mineral. Specifically for the Moon, differentiating among major minerals of interest using spectral parameters can be challenging due to overlapping diagnostic absorptions of distinct minerals in the 1 and 2 μm region (Figure 2). Through our calculation and testing of new parameters, we have supplemented the existing library of lunar mineral spectral parameters with the aim of improving upon the ability to detect lunar mineral spectral features of interest; for example, shifting from a band depth to integrated band depth parametrization given that the latter may be more noise resistant because more channels are used in the parameter calculation. We also acknowledge that the integrated band depth parametrization may be less specific about the wavelength of a particular absorption peak.

Calibration uncertainty is a separate factor that can influence I/F values and the spectral parameters from which they are derived (e.g., Rangarajan et al., 2024). M^3 on-orbit radiometric calibration was tested through comparison of the shape of M^3 Level 1b radiance data and radiance spectra from Apollo 16 returned soil samples. The Apollo 16 landing site imaged by M^3 was also used as a ground calibration site for radiometric calibration through comparison of a modeled radiance spectrum and the measured M^3 spectrum. Finally, an enhanced radiometric calibration validation was conducted through M^3 measurement comparison with United States Geological Survey RObotic Lunar Observatory (ROLO) measurements during which a search for similar observation geometries among the M^3 and ROLO data sets resulted in a good match at Mare Serenitatis. Subsequently, apparent reflectance measurements from M^3 and ROLO at Mare Serenitatis were compared and showed good agreement over the measured spectral range which was taken as a good initial validation of M^3 on orbit radiometric calibration (Green et al., 2011).

We also emphasize that the overlapping nature of OH and H_2O related absorptions in the 3-μm region, and the need to correct for thermal emission, may pose initial challenges in discerning the speciation of hydration on the lunar surface, and special care should be taken when interpreting the 3-μm feature. As such, we initially present the simple 3-μm integrated band depth (IBD3000) parameter to serve as a general indicator of potential hydration and flag key areas for further study. At the time of writing, we refrain from providing parameters (i.e., band depths at various isolated wavelengths) that may otherwise be misinterpreted as the presence or lack thereof of either H_2O or OH species. Additional water-related parameters can be further investigated upon future data set return to better suit the appropriate instrument; for example, revision of the wavelengths used to define the continuum for the IBD3000 parameter and, likely, a specific band position indicator to establish the variable forms of water.

The following techniques can aid in spectral parameter mineral identification limitations: the use of RGB parameter combinations, application of minimum threshold values to indicate the strongest spectral signatures, and verification of spectral parameter mineral indications with original reflectance spectra (Pelkey et al., 2007). Finally, the spectral parameters presented here are intended to serve as qualitative indicators of mineral spectral signature(s) (i.e., mineral and water indicator maps) to identify key areas for follow up investigations using spectra. We caution against direct parameter strength conversion to quantitative abundance because textural parameters and viewing geometry can also influence their magnitudes. Prior authors have estimated uncertainties in the values of three spectral parameters, presented to aid in pure water ice feature detection using multispectral High Resolution Imaging Science Experiment data at Mars, due to viewing geometry contributions and have

23335084, 2026, 3, Downloaded from https://agupubs.onlinelibrary.wiley.com/doi/10.1029/2025EA004557 by California Institute Of Tech, Wiley Online Library on [25/03/2026]. See the Terms and Conditions (https://onlinelibrary.wiley.com/terms-and-conditions) on Wiley Online Library for rules of use; OA articles are governed by the applicable Creative Commons License

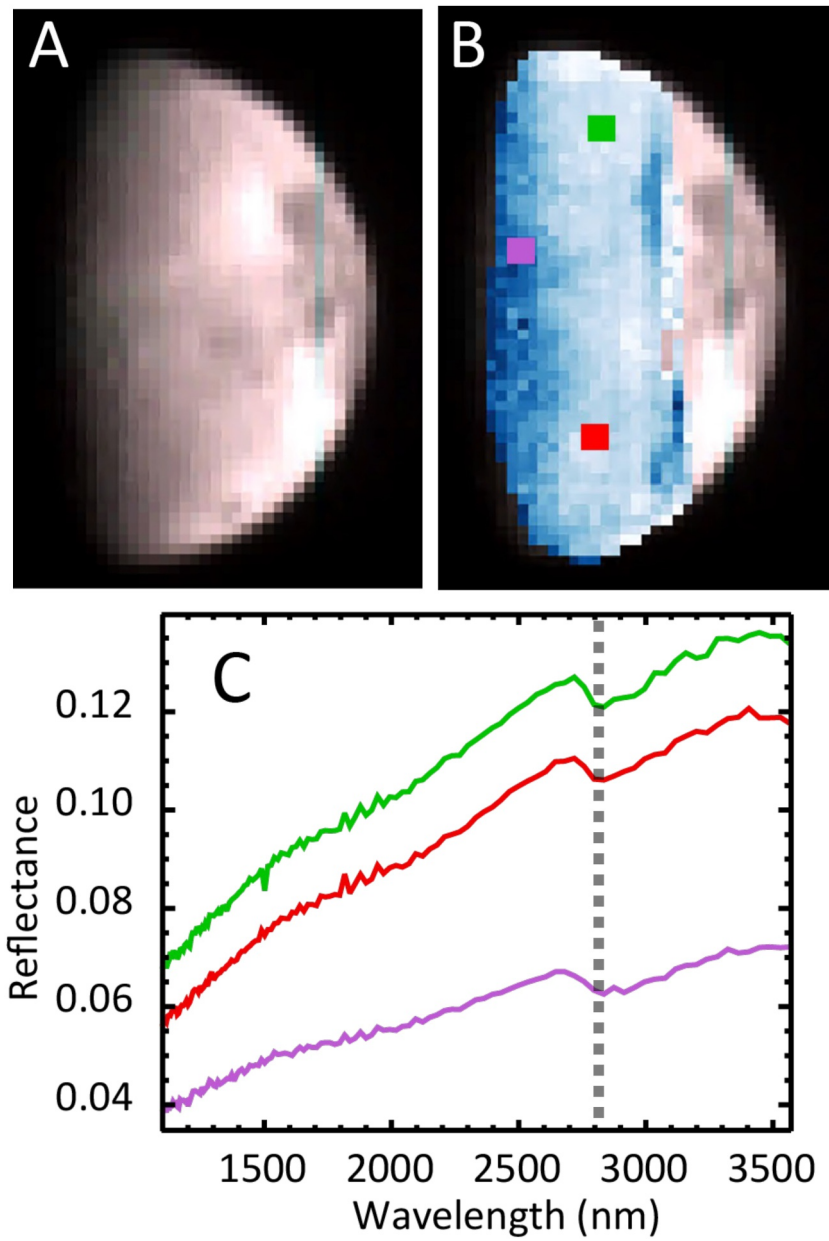


Figure 10. IBD3000 spectral parameter testing. (a) Deep Impact/EPOXI observation of the Moon on 05 December 2009 (day of year 339) and scan 01. (b) IBD3000 parameter map in blue, with color boxes correlating with spectra shown in (c). (c) Deep Impact/EPOXI spectra showing the 3-μm absorption feature with dashed line at ∼2.8 μm.

demonstrated that viewing geometry contributions to I/F cancel out for more simple spectral parameters but not for those considered more complicated (Rangarajan et al., 2024).

4. Conclusions

Global M^3 imaging spectrometer and Deep Impact/EPOXI data were used to formulate and test both mineral and water VSWIR spectral parameters for the Lunar Trailblazer HVM^3 instrument. Existing M^3 and newly formulated parameters can distinguish major lunar minerals alone, and in conjunction with one another as color composites. The newly presented IBD water parameter serves as a reliable indicator of hydration on the lunar surface. While the presented spectral parameters do have limitations, we show that overall they perform well and are valuable tools from which new information about lunar mineralogy and water presence could be derived when applied to

23335084, 2026, 3, Downloaded from https://agupubs.onlinelibrary.wiley.com/doi/10.1029/2025EA004557 by California Institute Of Tech, Wiley Online Library on [25/03/2026]. See the Terms and Conditions (https://onlinelibrary.wiley.com/terms-and-conditions) on Wiley Online Library for rules of use; OA articles are governed by the applicable Creative Commons License

23335084, 2026, 3, Downloaded from https://agupubs.onlinelibrary.wiley.com/doi/10.1029/2025EA004557 by California Institute Of Tech, Wiley Online Library on [25/03/2026]. See the Terms and Conditions (https://onlinelibrary.wiley.com/terms-and-conditions) on Wiley Online Library for rules of use; OA articles are governed by the applicable Creative Commons License

Lunar Trailblazer HVM^3 data, as well as for future lunar data sets similar to Trailblazer such as the UCIS-Moon instrument recently selected for a future orbital flight opportunity by NASA (Jet Propulsion Laboratory, 2025).

Conflict of Interest

The authors declare no conflicts of interest relevant to this study.

Data Availability Statement

M3Tools are publicly available on GitHub: https://github.com/nettlejw/M3Tools (Nettles, 2020).

HVM^3 thermal correction code be found at the Lunar Trailblazer github repository: https://github.com/LunarTrailblazr/HVM3-Thermal-Correction (Thompson, 2024).

HVM^3 parameter calculation code used for VNIR spectral parameters in this manuscript is deposited permanently on Zenodo (Dapremont, 2026).

EPOXI data set information can be found on the PDS: https://pds.nasa.gov/ds-view/pds/viewDataset.jsp?dsid=DIF-CAL-HRII-2-EPOXI-CALIBRATIONS-V2.0 (McLaughlin et al., 2011).

Acknowledgments
We thank the NASA Small Innovative Missions for Planetary Exploration (SIMPLEx) program and the entire Lunar Trailblazer team for their feedback and contribution to the efforts detailed here. The Lunar Trailblazer science team is funded via NASA contract 80MSFC19C0042 to Caltech. A portion of the research was carried out at the Jet Propulsion Laboratory, California Institute of Technology, under a contract with the National Aeronautics and Space Administration (80NM0019F0079). We thank an anonymous reviewer and Adrian Brown for comments that significantly improved the manuscript. We also thank the editor, Dr. Graziella Caprarelli.

References

Adams, J. B., & Goullaud, L. H. (1978). Plagioclase feldspars: Visible and near infrared diffuse reflectance spectra as applied to remote sensing. In *Lunar and Planetary Science Conference 9th* (pp. 2901–2909).

Adams, J. B., & McCord, T. B. (1970). Remote sensing of lunar surface mineralogy: Implications from visible and near-infrared reflectivity of Apollo 11 samples. In *Proceedings of the Apollo 11 Lunar Science Conference, in Geochimica et Cosmochimica Acta, Supplement* (Vol. 3, pp. 1937–1945).

Adams, J. B., Pieters, C., & McCord, T. B. (1974). Orange glass—Evidence for regional deposits of pyroclastic origin on the moon. In *Lunar Science Conference, 5th, Houston, Tex., March 18-22, 1974, Proceedings* (Vol. 1, pp. 171–186). Pergamon Press, Inc.

Bell, P. M., & Mao, H. K. (1973). Optical and chemical analysis of iron in Luna 20 plagioclase. *Geochimica et Cosmochimica Acta*, *37*(4), 755–758. https://doi.org/10.1016/0016-7037(73)90172-5

Bender, H. A., Smith, C. D., Ehlmann, B. L., Thompson, D. R., Vinckier, Q. P., & Mouroulis, P. (2022). Optical design and performance of the Lunar Trailblazer High-resolution Volatiles and Minerals Moon Mapper (HVM3). In *Proceedings of SPIE 12235, Imaging Spectrometry XXV: Applications, Sensors, and Processing* (p. 1223503). https://doi.org/10.1117/12.2632552

Besse, S., Sunshine, J., Staid, M., Boardman, J., Pieters, C., Guasqui, P., et al. (2013). A visible and near-infrared photometric correction for Moon Mineralogy Mapper (M^3). *Icarus*, *222*(1), 229–242. https://doi.org/10.1016/j.icarus.2012.10.036

Bishop, J. L. (2019). Visible and near-infrared reflectance spectroscopy: Laboratory spectra of geologic materials. In J. L. Bishop, I. I. I. J. F. Bell, & J. E. Moersch (Eds.), *Remote Compositional Analysis: Techniques for Understanding Spectroscopy, Mineralogy, and Geochemistry of Planetary Surfaces (Cambridge Planetary Science)* (pp. 68–101). Cambridge University Press.

Bishop, J. L., Pieters, C. M., & Edwards, J. O. (1994). Infrared spectroscopic analyses on the nature of water in montmorillonite. *Clays and Clay Minerals*, *42*(6), 702–716. https://doi.org/10.1346/CCMN.1994.0420606

Blue Origin. (2025). Blue origin and Luxembourg partner on Oasis-1 mission to map lunar resources. Retrieved from https://www.blueorigin.com/news/blue-origin-luxembourg-partner-on-oasis-1-mission

Boardman, J. W., Pieters, C. M., Green, R. O., Lundeen, S. R., Varanasi, P., Nettles, J., et al. (2011). Measuring moonlight: An overview of the spatial properties, lunar coverage, selenolocation, and related Level 1B products of the Moon Mineralogy Mapper. *Journal of Geophysical Research*, *116*, E00G14. https://doi.org/10.1029/2010JE003730

Bowles, N. E., Ehlmann, B. L., Klima, R. L., Calcutt, S., Donaldson Hanna, K. L., Edwards, C. S., et al. (2025). The lunar thermal mapper instrument for the lunar trailblazer mission. In *56th LPSC, abs #2382*.

Brown, A. J. (2025). Resolving asymmetric spectral bands. *Earth and Space Science*, *12*(3), e2024EA003981. https://doi.org/10.1029/2024EA003981

Burns, R. G. (1993). *Mineralogical applications of crystal field theory*. Cambridge University Press.

Calvin, W. M., & Clark, R. N. (1991). Modeling the reflectance spectrum of Callisto 0.25 to 4.1 μm. *Icarus*, *89*(2), 305–317. https://doi.org/10.1016/0019-1035(91)90180-2

Chauhan, M., Verma, P. A., & Chauhan, P. (2025). Level-2 processing of Chandrayaan-2 Imaging Infrared Spectrometer (IIRS) data for generation of surface reflectance. *Meteoritics & Planetary Science*, *60*(9), 2269–2282. https://doi.org/10.1111/maps.70037

Chauhan, P., Chauhan, M., Verma, P. A., Sharma, S., Bhattacharya, S., Dagar, A. K., et al. (2021). Unambiguous detection of OH and H_2O on the Moon from Chandrayaan-2 Imaging Infrared Spectrometer reflectance data using 3 μm hydration feature. *Current Science*, *121*(3), 391–401. https://doi.org/10.18520/cs/v121/i3/391-401

Cheek, L. C., Donaldson Hanna, K. L., Pieters, C. M., Head, J. W., & Whitten, J. L. (2013). The distribution and purity of anorthosite across the Orientale basin: New perspectives from Moon Mineralogy Mapper data. *Journal of Geophysical Research: Planets*, *118*(9), 1805–1820. https://doi.org/10.1002/jgre.20126

Clark, R. N., Pieters, C. M., Green, R. O., Boardman, J. W., & Petro, N. E. (2011). Thermal removal from near-infrared imaging spectroscopy data of the Moon. *Journal of Geophysical Research*, *116*, E00G16. https://doi.org/10.1029/2010JE003751

Clark, R. N. (1999). Spectroscopy of rocks and minerals and principles of spectroscopy. In A. N. Rencz & R. R. Ryerson (Eds.), *Remote Sensing for the Earth Sciences* (3rd ed., Vol. 3, pp. 3–58). John Wiley.

Clark, R. N. (2009). Detection of adsorbed water and hydroxyl on the Moon. *Science*, *326*(5952), 562–564. https://doi.org/10.1126/science.1178105

Clark, R. N., King, T. V. V., Klejwa, M., Swayze, G. A., & Vergo, N. (1990). High spectral resolution reflectance spectroscopy of minerals. *Journal of Geophysical Research*, *95*(B8), 12653–12680. https://doi.org/10.1029/JB095iB08p12653

Cloutis, E. A., Sunshine, J. M., & Morris, R. V. (2004). Spectral reflectance-compositional properties of spinels and chromites: Implications for planetary remote sensing and geothermometry. *Meteoritics & Planetary Sciences*, *39*(Nr 4), 545–565. https://doi.org/10.1111/j.1945-5100.2004.tb00918.x

Dapremont, A. M. (2026). M3Tools_HVM3 [Software]. *Zenodo*. https://doi.org/10.5281/zenodo.18175528

Donaldson Hanna, K. L., Cheek, L. C., Pieters, C. M., Mustard, J. F., Greenhagen, B. T., Thomas, I. R., & Bowles, N. E. (2014). Global assessment of pure crystalline plagioclase across the Moon and implications for the evolution of the primary crust. *Journal of Geophysical Research: Planets*, *119*(7), 1516–1545. https://doi.org/10.1002/2013JE004476

Ehlmann, B. L., Klima, R. L., Seybold, C. C., Klesh, A. T., Au, M. H., Bender, H. A., et al. (2022). IEEE Aerospace Conference (AERO), big sky (pp. 1–14). https://doi.org/10.1109/AERO53065.2022.9843663

Ehlmann, B. L., Klima, R. L., Seybold, C. C., Klesh, A. T., Bennett, C. L., Bowles, N., et al. (this issue). The Lunar Trailblazer Mission: Science motivation and implementation of a pioneering small satellite for lunar water and lunar geology in the NASA SIMPLEx program. *Journal of Geophysical Research*. https://doi.org/10.10/292025JE009300

Firefly Aerospace. (2025). Firefly aerospace announces new lunar imaging service on its elytra spacecraft. Retrieved from https://fireflyspace.com/news/firefly-aerospace-announces-new-lunar-imaging-service-on-its-elytra-spacecraft/

Gillis, J. J., & Lucey, P. G. (2004). Clementine 2.7 μm data: Mapping the mare and searching for water. In *35th LPSC, abs # 2158*.

Green, R. O., Pieters, C., Mouroulis, M., Eastwod, M., Boardman, J., Glavich, T., et al. (2011). The Moon Mineralogy Mapper (M3) imaging spectrometer for lunar science: Instrument description, calibration, on-orbit measurements, science data calibration and on-orbit validation. *Journal of Geophysical Research*, *116*, E00G19. https://doi.org/10.1029/2011JE003797

Hampton, D. L., Baer, J. W., Huisjen, M. A., Varner, C. C., Delamere, A., Wellnitz, D. D., et al. (2005). An overview of the instrument suite for the deep impact mission. *Space Science Reviews*, *117*(1–2), 43–93. https://doi.org/10.1007/s11214-005-3390-8

Hapke, B. (1993). *Theory of reflectance and emittance spectroscopy*. Cambridge University Press.

Hawke, B. R., Peterson, C. A., Blewett, D. T., Bussey, D. B. J., Lucey, P. G., Taylor, G. J., & Spudis, P. D. (2003). Distribution and modes of occurrence of lunar anorthosite. *Journal of Geophysical Research*, *108*(E6), 5050. https://doi.org/10.1029/2002JE001890

Heiken, G., Vaniman, D., & French, B. M. (1991). *Lunar sourcebook: A user's guide to the Moon*. Cambridge University Press.

Isaacson, P. J., Pieters, C. M., Besse, S., Clark, R. N., Head, J. W., Klima, R. L., et al. (2011). Remote compositional analysis of lunar olivine-rich lithologies with Moon Mineralogy Mapper (M3) spectra. *Journal of Geophysical Research*, *116*, E00G11. https://doi.org/10.1029/2010JE003731

Jet Propulsion Laboratory. (2025). NASA's lunar trailblazer Moon mission ends. Retrieved from https://www.nasa.gov/missions/small-satellite-missions/lunar-trailblazer/nasas-lunar-trailblazer-moon-mission-ends/

Kieffer, H. H. (1995). A spectral search for H_2O near the lunar North pole. *Bulletin of the American Astronomical Society*, *27*, 1110.

Klima, R., Cahill, J., Hagerty, J., & Lawrence, D. (2013). Remote detection of magmatic water in Bullialdus crater on the Moon. *Nature Geoscience*, *6*(9), 737–741. https://doi.org/10.1038/ngeo1909

Klima, R. L., Pieters, C. M., Boardman, J. W., Green, R. O., Head, J. W., Isaacson, P. J., et al. (2011). New insights into lunar petrology: Distribution and composition of prominent low-Ca pyroxene exposures as observed by the Moon Mineralogy Mapper (M3). *Journal of Geophysical Research*, *116*, E00G06. https://doi.org/10.1029/2010JE003719

Kramer, G. Y., Besse, S., Nettles, J., Combe, J.-P., Clark, R. N., Pieters, C. M., et al. (2011). Newer views of the Moon: Comparing spectra from Clementine and the Moon Mineralogy Mapper. *Journal of Geophysical Research*, *116*, E00G04. https://doi.org/10.1029/2010JE003728

Kramer, G. Y., Kring, D. A., Nahm, A. L., & Pieters, C. M. (2013). Spectral and photogeologic mapping of Schrödinger Basin and implications for post-South Pole-Aitken impact deep subsurface stratigraphy. *Icarus*, *223*(1), 131–148. https://doi.org/10.1016/j.icarus.2012.11.008

Laferriere, K. L., Sunshine, J. M., & Feaga, L. M. (2022). Variability of hydration across the southern hemisphere of the Moon as observed by Deep Impact. *Journal of Geophysical Research: Planets*, *127*(8), e2022JE007361. https://doi.org/10.1029/2022JE007361

Li, S., Lucey, P. G., Milliken, R., Hayne, P., Fisher, E., Williams, J. P., et al. (2018). Direct evidence of surface exposed water ice in the lunar polar regions. *Proceedings of the National Academy of Sciences*, *115*(36), 8907–8912. https://doi.org/10.1073/pnas.1802345115

Li, S., & Milliken, R. E. (2017). Water on the surface of the Moon as seen by the Moon Mineralogy Mapper: Distribution, abundance, and origins. *Science Advances*, *3*(9), e1701471. https://doi.org/10.1126/sciadv.1701471

Lucey, P., Korotev, R. L., Gillis, J. J., Taylor, L. A., Lawrence, D., Campbell, B. A., et al. (2006). Understanding the lunar surface and Space-Moon interactions. *Reviews in Mineralogy and Geochemistry*, *60*(1), 83–219. https://doi.org/10.2138/rmg.2006.60.2

Matsunaga, T., Ohtake, M., Haruyama, J., Ogawa, Y., Nakamura, R., Yokota, Y., et al. (2008). Discoveries on the lithology of lunar crater central peaks by SELENE Spectral Profiler. *Geophysical Research Letters*, *35*(23), L23201. https://doi.org/10.1029/2008GL035868

McLaughlin, S. A., Carcich, B., Sackett, S. E., Klaasen, K. P., & Wellnitz, D. D. (2011). Epoxi inflight calibrations—HRII RAW SPECTRA V2.0, DIF-CAL-HRII-2-EPOXI-CALIBRATIONS-V2.0 [Dataset]. *NASA Planetary Data System*. https://pds.nasa.gov/ds-view/pds/viewDataset.jsp?dsid=DIF-CAL-HRII-2-EPOXI-CALIBRATIONS-V2.0

Milliken, R. E., & Li, S. (2017). Remote detection of widespread indigenous water in lunar pyroclastic deposits. *Nature Geoscience*, *10*(8), 561–565. https://doi.org/10.1038/ngeo2993

Mustard, J. F., Pieters, C. M., Isaacson, P. J., Head, J. W., Besse, S., Clark, R. N., et al. (2011). Compositional diversity and geologic insights of the Aristarchus crater from Moon Mineralogy Mapper data. *Journal of Geophysical Research*, *116*, E00G12. https://doi.org/10.1029/2010JE003726

Nettles, J. W. (2020). M3Tools [Software]. Retrieved from https://github.com/nettlejw/M3Tools

Ohtake, M., Matsunaga, T., Haruyama, J., Yokota, Y., Morota, T., Honda, C., et al. (2009). The global distribution of pure anorthosite on the Moon. *Nature*, *461*(7261), 236–240. https://doi.org/10.1038/nature08317

Pelkey, S. M., Mustard, J. F., Murchie, S., Clancy, R. T., Wolff, M., Smith, M., et al. (2007). CRISM multispectral summary products: Parameterizing mineral diversity on Mars from reflectance. *Journal of Geophysical Research*, *112*(E8), E08S14. https://doi.org/10.1029/2006JE002831

Pieters, C. M., Klima, R. L., & Green, R. O. (2019). Compositional analysis of the Moon in the visible and near-infrared regions. In J. Bishop, J. Bell III., & J. Moersch (Eds.), *Remote Compositional Analysis: Techniques for Understanding Spectroscopy, Mineralogy, and Geochemistry of Planetary Surfaces (Cambridge Planetary Science)* (pp. 368–392). Cambridge: Cambridge University Press. https://doi.org/10.1017/9781316888872.020

Pieters, C. M., Besse, S., Boardman, J., Buratti, B., Cheek, L., Clark, R. N., et al. (2011). Mg spinel lithology:A new rock type on the lunar farside. *Journal of Geophysical Research*, *116*, E00G08. https://doi.org/10.1029/2010JE003727

23335084, 2026, 3, Downloaded from https://agupubs.onlinelibrary.wiley.com/doi/10.1029/2025EA004557 by California Institute Of Tech, Wiley Online Library on [25/03/2026]. See the Terms and Conditions (https://onlinelibrary.wiley.com/terms-and-conditions) on Wiley Online Library for rules of use; OA articles are governed by the applicable Creative Commons License

Pieters, C. M., Boardman, J., Buratti, B., Clark, R., Combe, J. P., Green, R., et al. (2009). Mineralogy of the lunar crust in spatial context: First results from the Moon Mineralogy Mapper (M3). In *40th LPSC, abs #2052*.

Pieters, C. M., Goswami, J. N., Clark, R. N., Annadurai, M., Boardman, J., Buratti, B., et al. (2009). Character and spatial distribution of OH/H_2O on the surface of the Moon seen by M^3 on Chandrayaan-1. *Science*, *326*(5952), 568–572. https://doi.org/10.1126/science.1178658

Pieters, C. M., Hanna, K. D., Cheek, L., Dhingra, D., Prissel, T., Jackson, C., et al. (2014). The distribution of Mg-spinel across the Moon and constraints on crustal origin. *American Mineralogist*, *99*(10), 1893–1910. https://doi.org/10.2138/am-2014-4776

Pieters, C. M., Head, J. W., Adams, J. B., McCord, T. B., Zisk, S. H., & Whitford Stark, J. L. (1980). Late high titanium basalts of the western Maria: Geology of the Flamsteed region of Oceanus Procellarum. *Journal of Geophysical Research*, *85*(B7), 3913–3938. https://doi.org/10.1029/jb085ib07p03913

Rangarajan, V. G., Tornabene, L. L., Osinski, G. R., Dundas, C. M., Beter, R. A., Herkenhoff, K. E., et al. (2024). Novel quantitative methods to enable multispectral identification of high-purity water ice exposures on Mars using High Resolution Imaging Science Experiment (HiRISE) images. *Icarus*, *419*, 115849. https://doi.org/10.1016/j.icarus.2023.115849

Rodgers, C. D. (2000). Inverse methods for atmospheric sounding: Theory and practice. In *World Scientific* (Vol. 2).

Sodha, G., & Dhingra, D. (2025). Novel geological framework to understand the origin and diversity of orthopyroxene, olivine, spinel (OOS) lithologies on the Moon. *Scientific Reports*, *15*(1), 2426. https://doi.org/10.1038/s41598-025-86248-9

Staid, M. I., & Pieters, C. M. (2001). Mineralogy of the last lunar basalts: Results from clementine. *Journal of Geophysical Research*, *106*(E11), 27887–27900. https://doi.org/10.1029/2000JE001387

Staid, M. I., Pieters, C. M., Besse, S., Boardman, J., Dhingra, D., Green, R., et al. (2011). The mineralogy of late stage lunar volcanism as observed by the Moon Mineralogy Mapper on Chandrayaan 1. *Journal of Geophysical Research*, *116*, E00G10. https://doi.org/10.1029/2010JE003735

Sun, Y., Li, L., & Zhang, Y. (2017). Detection of Mg-spinel bearing central peaks using M3images: Implications for the petrogenesis of Mg-spinel. *Earth and Planetary Science Letters*, *465*, 48–58. https://doi.org/10.1016/j.epsl.2017.01.019

Sunshine, J. M., Farnham, T. L., Feaga, L. M., Groussin, O., Merlin, F., Milliken, R. E., & A'Hearn, M. F. (2009). Temporal and spatial variability of lunar hydration as observed by the Deep Impact spacecraft. *Science*, *326*(5952), 565–568. https://doi.org/10.1126/science.1179788

Tarantola, A. (2005). *Inverse problem theory and methods for model parameter estimation*. Society for Industrial and Applied Mathematics.

Thompson, D. R. (2024). HVM3-thermal-correction [Software]. Retrieved from https://github.com/LunarTrailblazr/HVM3-Thermal-Correction

Thompson, D. R., Ehlmann, B. L., Green, R. O., Allen, G. D., Bender, H., Copley-Woods, D., et al. (this issue). Calibration and performance of the high-resolution volatiles and minerals Moon mapper (HVM^3). *Earth and Space Science*. https://doi.org/10.1029/2025EA004456

Thompson, D. R., Natraj, V., Green, R. O., Helmlinger, M. C., Gao, B. C., & Eastwood, M. L. (2018). Optimal estimation for imaging spectrometer atmospheric correction. *Remote Sensing of Environment*, *216*, 355–373. https://doi.org/10.1016/j.rse.2018.07.003

Tompkins, S., & Pieters, C. M. (2010). Spectral characteristics of lunar impact melts and inferred mineralogy. *Meteoritics & Planetary Sciences*, *45*(7), 1152–1169. https://doi.org/10.1111/j.1945-5100.2010.01074.x

Viviano, C. E., Seelos, F. P., Murchie, S. L., Kahn, E. G., Seelos, K. D., Taylor, H. W., et al. (2014). Revised CRISM spectral parameters and summary products based on the currently detected mineral diversity on Mars. *Journal of Geophysical Research: Planets*, *119*(6), 1403–1431. https://doi.org/10.1002/2014JE004627

Yamamoto, S., Nakamura, R., Matsunaga, T., Ogawa, Y., Ishihara, Y., Morota, T., et al. (2010). Possible mantle origin of olivine around lunar impact basins detected by SELENE. *Nature Geoscience*, *3*(8), 533–536. https://doi.org/10.1038/ngeo897

23335084, 2026, 3, Downloaded from https://agupubs.onlinelibrary.wiley.com/doi/10.1029/2025EA004557 by California Institute Of Tech, Wiley Online Library on [25/03/2026]. See the Terms and Conditions (https://onlinelibrary.wiley.com/terms-and-conditions) on Wiley Online Library for rules of use; OA articles are governed by the applicable Creative Commons License